CONTROL OF QUADRUPED WALKING BEHAVIOR THROUGH AN EMBEDDING OF SPRING LOADED INVERTED PENDULUM TEMPLATE

A THESIS SUBMITTED TO
THE GRADUATE SCHOOL OF NATURAL AND APPLIED SCIENCES
OF
MIDDLE EAST TECHNICAL UNIVERSITY

BY

MERT KAAN YILMAZ

IN PARTIAL FULFILLMENT OF THE REQUIREMENTS
FOR
THE DEGREE OF MASTER OF SCIENCE
IN
COMPUTER ENGINEERING

AUGUST 2022

Approval of the thesis:

CONTROL OF QUADRUPED WALKING BEHAVIOR THROUGH AN EMBEDDING OF SPRING LOADED INVERTED PENDULUM TEMPLATE

submitted by **MERT KAAN YILMAZ** in partial fulfillment of the requirements for the degree of **Master of Science in Computer Engineering Department, Middle East Technical University** by,

Prof. Dr. Halil Kalıpçılar
Dean, Graduate School of **Natural and Applied Sciences** ________________

Prof. Dr. Halit Oğuztüzün
Head of Department, **Computer Engineering** ________________

Prof. Dr. Uluç Saranlı
Supervisor, **Computer Engineering, METU** ________________

Examining Committee Members:

Assist. Prof. Dr. Yıldıray Yıldız
Mechanical Engineering, Bilkent University ________________

Prof. Dr. Uluç Saranlı
Computer Engineering, METU ________________

Assist. Prof. Dr. İsmail Uyanık
Electrical and Electronics Engineering, Hacettepe University ________________

Date: 08.09.2022

I hereby declare that all information in this document has been obtained and presented in accordance with academic rules and ethical conduct. I also declare that, as required by these rules and conduct, I have fully cited and referenced all material and results that are not original to this work.

Name, Surname: Mert Kaan Yılmaz

Signature :

ABSTRACT

CONTROL OF QUADRUPED WALKING BEHAVIOR THROUGH AN EMBEDDING OF SPRING LOADED INVERTED PENDULUM TEMPLATE

Yılmaz, Mert Kaan
M.S., Department of Computer Engineering
Supervisor: Prof. Dr. Uluç Saranlı

August 2022, 54 pages

Legged robots require complex dynamical behaviours in order to achieve stable, sustainable and efficient locomotion. Due to their mobile nature, they can neither afford to provide extensive computational power, nor use anything but the most energy efficient structural designs and algorithms to achieve stability and speed. Consequently, simple and efficient ways to solve the complex set of problems is one of the key points of focus in legged robot locomotion research. This thesis offers a novel method that uses an active embedding of the Spring-Loaded Inverted Pendulum (SLIP) dynamical model within a planar quadruped model in order to reduce the complexity of the control problem while also keeping the overall locomotion as efficient as possible. In particular, we hypothesize that the embedding of the SLIP model is particularly effective when used in conjunction with legs that incorporate compliance in parallel with the traditionally fully-actuated leg structures in most modern quadruped platforms. We first show in simulation, using a planar quadruped model with fully actuated 2DOF legs, how the embedding of the SLIP model is performed, and compare the locomotion performance with other contemporary methods. Subsequently, we show that the leg force profiles that arise from this embedding can largely be generated passively with the incorporation of parallel leg compliance during steady-state running, with only a small amount of energy expenditure necessary during stance to achieve stability and compensation of losses. We also provide comparative results to illustrate the efficiency of this approach for potential platforms with parallel compliance incorporated into the leg structure.

Keywords: Legged robots, quadruped, locomotion control, energy efficiency, spring-loaded inverted pendulum, template-based control

ÖZ

DÖRT BACAKLI ROBOTLARDA YÜRÜME DAVRANIŞININ GÖMÜLMÜŞ BİR YAYLI TERS SARKAÇ ŞABLONU İLE KONTROLÜ

Yılmaz, Mert Kaan
Yüksek Lisans, Bilgisayar Mühendisliği Bölümü
Tez Yöneticisi: Prof. Dr. Uluç Saranlı

Ağustos 2022 , 54 sayfa

Bacaklı robotlar, istikrarlı, sürdürülebilir ve verimli hareket elde etmek için kompleks dinamik davranışlar gerektirir. Mobil yapıları nedeniyle, ne yüksek kapasitede hesaplama gücü kullanabiliyor ne de denge ve hız elde etmek için enerji açısından en verimli yapısal tasarımlar ve algoritmalar dışında hiçbir şey kullanamıyor olmaları sebebiyle, karmaşık problem setini çözmenin basit ve etkili yolları, bacaklı robot hareket araştırmalarında odak noktalarından biridir. Bu tez, kontrol probleminin karmaşıklığını azaltmak ve aynı zamanda genel hareketi mümkün olduğunca verimli tutmak için Yaylı Ters Sarkaç dinamik modelinin düzlemsel dört bacaklı bir model içine aktif bir şekilde yerleştirilmesini kullanan yeni bir yöntem sunmaktadır. Özellikle, SLIP modelinin gömülmesinin, çoğu modern dört bacaklı platformda bacak yapılarına paralel olarak uyumu içeren bacaklar ile birlikte kullanıldığında özellikle etkili olduğunu varsayıyoruz. İlk önce, 2 özgürlük derecine sahip bacakları olan düzlemsel dört bacaklı bir model kullanarak simülasyonda, Yaylı Ters Sarkaç modelinin yerleştirilmesinin nasıl yapıldığını gösteriyoruz ve hareket performansını diğer çağdaş yöntemlerle karşılaştırıyoruz. Daha sonra, bu gömülmeden kaynaklanan bacak kuvveti profillerinin, kararlı durum çalışması sırasında paralel bacak uyumunun dahil edilmesiyle büyük ölçüde pasif olarak üretilebileceğini ve duruş sırasında stabilite ve kayıpların telafisi için gerekli olan sadece küçük bir miktarda enerji harcaması gerektiğini gösterdik. Bacak yapısına paralel uyumluluğa sahip potansiyel platformlar için bu yaklaşımın etkinliğini göstermek için karşılaştırmalı sonuçlar da sunuyoruz.

Anahtar Kelimeler: Bacaklı robotlar, dört bacaklı robotlar, yürüyüş kontrolü, enerji verimliliği, yaylı ters sarkaç, kalıp temelli kontrol

I dedicate this to my wife, who was always there for me.

ACKNOWLEDGMENTS

I could not have undertaken this journey without my professor, who generously provided knowledge and expertise.

I should mention my wife who was my girlfriend back then when I embarked on this adventure. She was always by my side.

I would be remiss in not mentioning my family, especially my parents. Their belief in me has kept my spirits and motivation high during this process.

I would also like to thank my cat who joined our family towards the end for all the entertainment and emotional support.

TABLE OF CONTENTS

CHAPTERS

LIST OF TABLES

TABLES

LIST OF FIGURES

FIGURES

CHAPTER 1

INTRODUCTION

1.1 Motivation and Problem Definition

In recent years, legged robots have received an increasing amount of attention in robotics research. Even though many robust and efficient wheeled and tracked robots do exist [1, 2], lack of stable movement through unstructured terrain in wheeled robots makes legged robots a compelling alternative for many use cases [3]. In harmful circumstances where humans cannot be at the scene, a robust legged robot can make sure that no extra lives are at risk [4, 5].

Limited by the current mechanical/computational state of the art, many research groups focus on finding locomotion control methods that are both efficient and effective [6, 7, 8]. Recent legged robots have much higher number of degrees of freedom as compared to older platforms that were limited by available components and manufacturing constraints [9, 10]. This means that more complex control methods are required to make sure that no energy is wasted during locomotion [11, 12]. It has been the latest trend to take advantage of increasing computational power in the processing units to solve these complex problems [13, 14]. However, even now, solving full body dynamics is not yet a feasible approach to this problem. Use of new highly efficient motors still cannot compensate what control methods lack in that regard [15, 16].

To grasp the underlying dynamics of the locomotion behavior, nature has always been a starting point [17, 18]. Years of study on the animals and humans has shown that many of the animal locomotion contains similarities, which helps us reduce the model to its core components [19, 20]. "Spring Loaded Inverted Pendulum"(SLIP) is one of the models which greatly reduces the effort to control the system [21] where in this model, even though this model merely consist of a mass and a spring, it can capture the highly complex dynamics of animals, humans or robots. All that's left for controllers is to either embed this model as a high level controller or make our robots closer to this model [7, 8]. Embedding SLIP to the controller is a more common approach, since we may not be able to change the physical state of the robots [22, 23]. However, the improvements in parallel compliance is showing promising results [24]. Both of these approaches make sure that the robots keep the desired characteristics of the behavior while preserving natural stable gait of locomotion [25].

A combination of a controller that has embedded SLIP and a mechanical leg design that takes advantage of parallel compliance would result in the most animal-like locomotion behavior observed in the nature. This thesis takes another step by creating an instance of this controller and showing the efficiency of the locomotion if a quadruped to use this approach.

1.2 Contributions and Novelties

In this thesis, a high level controller for SLIP and a low level controller where SLIP is embedded to fully control the quadruped is used. Hence, high level controller oversee the speed and jump height of the robot, while low level controller takes advantage of embedded SLIP to solve the inverse dynamics to keep the stability. Not only that, but the these controllers together takes advantage of the parallel compliancy at the legs of the robot.

To keep the problem simpler, a planar version of quadruped has been used to show the controller. This controller aims to reduce the problems size by numerous times, while keeping the stable gait thanks to its complementary dynamics of SLIP. This controller is tested on a simulation where the only inputs to the system are the torques to the motors of quadruped. Moreover, its efficiency is compared between Linear Inverted Pendulum(LIP) embedded controller, SLIP embedded controller and SLIP embedded controller with parallel compliancy at the legs.

1.3 The Outline of the Thesis

Chapter 2 is giving all the needed background, starting from the nature of locomotion. Crucial SLIP related studies shall also be introduced here. The last bit of this chapter is about contemporary quadruped designs and control methods.

In Chapter 3, template models methods are deeply investigated. Kicking off with design choices, model and dynamics of both SLIP and LIP, delineating the embedding controllers of each respective model are also done here.

Chapter 4 starts with the planar quadruped model used to embed template models on. The model details, dynamics and control problems are addressed here. First, the LIP embedded control method is introduced. Next, the SLIP embedded model is elaborated.

Chapter 5 gives clear examples of three different controllers, shows their convergence to a stable gait, compares them with each other in terms of efficiency and draws conclusions.

In chapter 6, the resolutions agreed from all the chapters are discussed briefly, verdicts are cleared and limitations of the work is considered. Future work that can be done to improve the methods are also here.

CHAPTER 2

BACKGROUND

2.1 Nature of Locomotion

The nature has always been a starting point for the problems in the physical world. Running motions of the horse and cheetah were deeply investigated in [17], while comparing similarities and differences between each other. Authors have also claimed that they have observed a measuring-worm like motion. Conclusions are stated on why cheetah's stride is relatively longer than horse, such as having longer suspension in flight, two principal suspension periods instead of one, etc. In another article, [18], it is addressed that how the step length and limb speed during galloping and slower stepping is effected in cats. In both articles, authors tried to draw conclusions from nature so that they can understand the underlying principle behind the locomotion.

Although mobile robots with wheels quite popular during the days that these articles are written, in [3], the author states that in terrestrial environments, rotating systems are feasible as a form of transportation only on relatively flat, open terrain and become less useful as the size of the rotating element decreases. The relationship between wheel diameter and the height of obstacles which can be surmounted poses serious limitations for the utility of wheels as a general mode of transportation. Whenever rotating systems are a feasible mode of transportation, organisms have evolved that use these systems.

One of the most revolutionary research on legged locomotion was [26]. It was done using a planar one-legged hopper that can actively balance. A quadruped with trotting performance is demonstrated. Symmetry is stated as an important aspect of simplification of locomotion, and heuristical approaches have been made for developing of algorithms in locomotion behaviors. Control of running decomposed into parts, which also applies for multiple dimensions. Following the success of this article, many articles published on the nature of locomotion. In [27], the effects of compliance in running animals and robots are investigated. Springs in robots, tendons in animals are claimed to help with the energy savings, reduce unwanted heat production and provide stability through preventing chatter/noise from the touchdown. Article starts from animals and build ideas for robots upon that.

In another article, [28], interpretation and analysis of robots that walks without any input or energy injection provided that they are in a desired initial condition such as a slope. Dynamics of the robots are analyzed and robot in different perturbations are tested. the simplest model of running is presented in [29] with just a mass, spring and parameters such as stride length and peak ground reaction force. Parameters are tested with experimental data from literature, and it shows that in high forward speed, leg stiffness is linearly related to forward speed and vertical speed.

2.2 Template Models

By observing energy-like quantities, the authors of [20] found out that there is a discrete dynamical system between the model and the collision between robot and environment. Using the vertical hopper with the Raibert's controller from [26], authors have shown an insight to existence of a high level model for the control of this kind of robotics tasks. Also in [19], the authors' analysis showed that vertical ground reaction force and vertical compression did not depend on body mass. Even with different dynamics, there were comparable energetics of the center of mass. This results in decrease of natural frequency with body mass. Using high stiffness legs, small animals can provide more stable gaits. All in all, these findings show that monopode is a very universal model for legged terrestrial locomotion.

Another work that was born from Raibert's work was [8]. A planar one legged robot has been assembled and controlled with Raibert's control laws. Authors have concluded that mechanical solutions had to go with the controller solutions and even though the robot was the best energetic performing robot by that time, it can get even better by implementing a passive running with a hip compliance.

At this point, authors were trying to find a high level model to reduce the computational power required during the locomotion. One of the most important work on is done In [21]. Here, authors present a template which is made to resolve the redundancy of multiple legs, joints and muscles by seeking synergies and symmetries. More elaborate models are named as anchors where more detailed models are described such as joint torques, neural systems etc. The idea is to start from a template, use it as an overseer of control, then add several degrees of freedom to couple both mechanisms. The mechanical system gives passive self-stabilization and the neural system provides slow but active stabilization.

Starting with the high dimensional problem of stability analysis of bipeds, In [30], authors provide a model for collapsing the dimensions to the one dimensional-set and using Poincare analysis on it. Also, zero dynamics of the biped was not invariant, however, it can be recovered with high gain control. Another work was [7], where a hexapod robot with compliant legs are designed to demonstrate stable walking over rough terrain. Using an open-loop controller, three legs are driven simultaneously in a tripod kind of behavior. Although authors were not able to provide a mathematically informed analysis of reasons for robots' movement, empirical results of these behaviors are shown. Moreover, building upon the RHex work, in [31], two new behaviors that utilizes feedback from the environment are introduced. This controller is adapted to handle sloped terrain and run even more efficiently through synchronizing the natural frequency of the mechanical system with the controller.

As SLIP is more and more researched, better solvers were introduced. In [22], by presenting a precise yet approximate solution to SLIP with damping included, authors were able to drop the average predictive error below %2. Also, a gait-level running controller were designed by taking advantage of this solution method. This resulted in even more precise embeddings of SLIP model to the real systems. In [32], pronking behavior is shown on a planar hexapod robot with compliant legs utilizing template based control. Here, high level control is regulated through SLIP model and embedding controller provides stability of the robot gait.

In [23], a novel controller is presented to lessen the power requirements and increase the energy input in a single step of the system for the linearly actuated compliant leg systems. The SLIP template is a lossy one with a tunable damping coefficient to the leg system. Hence, the new controller provides more stable and efficient tracking of gait template for linearly actuated compliant leg systems. One of the more recent work is build upon the decoupled nature of SLIP. In [16], the authors have build a 12DoF passive compliant legged robot with four motors, and they have demonstrated a number of different tasks with it. From the application in parallel of four simple, completely decoupled 1DoF feedback laws represents some simple but crucial specific component of the locomotion task at hand to realize the behavior.

2.3 Quadrupeds

Although the quadruped history is believed to start around 400 million years ago in world history, one of the oldest article on quadruped robots in modern world is [6]. To test many gait types, a quadruped robot was used, and a single control algorithm was responsible for derivation of different gait types with simple parameter variation. With hydraulic actuators and 2 degrees of freedom in hips, the four-legged robot was able to perform trotting, pacing and bounding while also keeping stability between transitions of these gaits. After several years, in [33], a quadruped with just a single degree of freedom in each leg and a mechanical switch for ground detection is introduced. This mechanical simplicity makes it cheaper and more reliable. Motors are RC servos and the robot was able to perform walk, turn, step climb, stair climb and running behavior.

In [34], BigDog has onboard systems that provide power, actuation, sensing, controls and communications and the robot's power comes from a combustion engine. Each leg has 4 hydraulic actuators that power the joints, as well as a 5th passive degree of freedom that is provided with a spring on the leg. BigDog is quite noisy and power hungry, thanks to its combustion engine design.

As electrical motors become more and more common, quadruped designs also started to evolve towards using them. In [9], design principles and analysis of MIT Cheetah robot are stated, and these principles are derived from energy losses from running behavior. With their solutions to the stated problems, robot is built and was able to demonstrate fast trotting behavior with deep analysis of energy efficiency. At this point, there were still novel hydraulically actuated robots were designed, such as [35]. This robot was able to demonstrate behaviors such as self-rightening, stair climbing, etc. A meticulous research is done on optimizing actuator areas, and the article itself is a deep cover of hydraulically actuated robots.

One of the most impacting works on quadruped design were [36]. Born from high engineering, MIT Cheetah 3 deployed with a new leg design that leverages high bandwidth proprioceptive actuators. The robot is shown to have a very low cost of transport and with the help of the novel controller, the robot is able to blindly climb stairs. It was also low-cost, which meant that many researchers around the globe can create theirs own quadrupeds with ease. Some other groups also created their own open source quadruped designs, such as [37]. This robot that utilizes low gear ratio DC motors with 3D printable and off-the-shelf parts is designed to be distributed in masses inexpensively. The robot demonstrates with a controller that combines feedforward contact forces computed from a kino-dynamic optimizer with impedance control of the center of mass and base orientation.

2.4 Quadruped Control Methods

As the design of quadruped was iteratively getting better, control of these quadruped designs are fairly new topic. High degree of freedom of quadrupeds with small time period to compute a meaningful action makes them hard to control robots. However, In [11], a model predictive control(MPC) implementation is used to predict the ground reaction forces. A simplified version of the robot model that captures the whole 3D dynamics is in the core of the system to formulate the convex optimization. Demonstrations of stand, trot, flying-trot, pace and many other behaviors are shown meticulously. In [15], building upon [11] and using the MPC model that predicts the reaction forces of legs introduced in that article, this new controller combines Whole Body Control(WBC) with MPC to compute joint torques, position and velocity commands based on optimal reaction forces that are computed from the MPC. A number of different gaits are presented on MIT Mini-Cheetah with this novel controller.

In [12], using two fundamental component, the authors were able to create a novel strategy for when there is only on-board mapping for terrain morphology. First a safe foothold location is found using convolutional neural networks and then a model predictive control method is used to find optimal reaction forces for the found foothold locations. This strategy is tested on hydraulically actuated HyQReal quadruped robot.

Another controller was shown in [10]. Similar to [11], an MPC that is based on the centroidal dynamics, which computes desired optimal reaction forces for the sake of following the reference velocity. With differing at state estimation and whole body controller, this novel controller is tested on the reliable low-cost robot SOLO-12.

One of the latest works includes learning methods, such as [14]. Using reinforcement learning that is trained for contact schedules of each foot while MPC optimizes motor torques to make robot walk in the desired velocity. This novel framework is shown to be performing well with automatic gait transitions from walking to fly-trotting. Moreover, it is stated that energy efficiency is higher for a wide range of locomotion speed than baseline controllers.

CHAPTER 3

TEMPLATE MODELS

3.1 The Linear Inverted Pendulum Template

Linear inverted pendulum(LIP) model is used in robotics as a high-level trajectory model [38, 39, 40]. This model aims to keep the height of the center of mass constant throughout the motion and tries to control the velocity of the system. LIP has been adopted by many researchers as it is a very simple model that doesn't require approximate solutions for the center of mass trajectory [41, 42]. There have been researches on its stability and efficiency, which proves LIP as a powerful and easy-to-use model under disposal [43, 44].

3.1.1 System Model and Dynamics

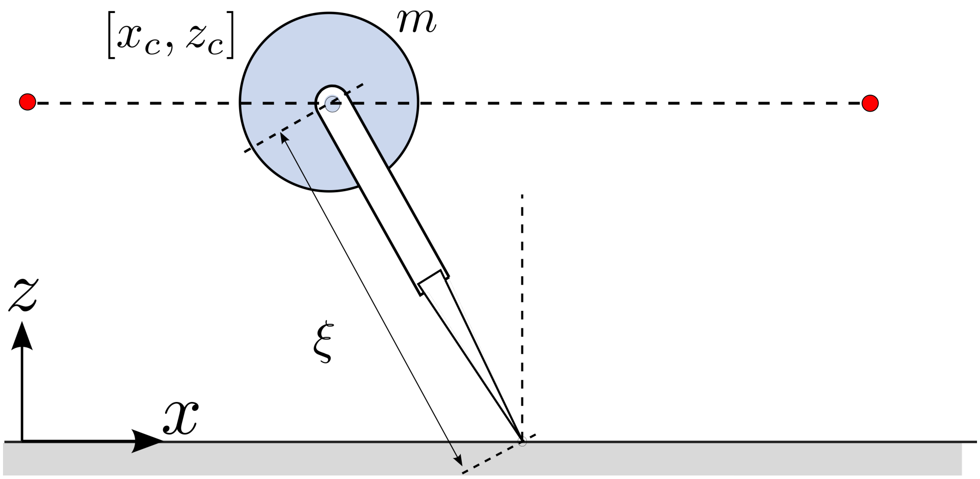

Figure 3.1: LIP Model and related parameters

An illustration of the model can be seen in figure 3.1. Here, we can witness how the

Variable	Definition
$[x_c, z_c]$	LIP CoM of body position (in W)
$[z_d, \dot{x_d}]$	Desired LIP CoM height and velocity (in W)
m	Total body mass

Table 3.1: Parameters of the LIP model

model tries to keep the CoM above the desired target. The legs of the model, in this case, can be imagined as a linear motor that changes with the position of the CoM. The parameters of the model can also be identified at the table 3.1.

LIP model either does not have flight phase. This is because to keep the CoM on a horizontal axis, there has to be a constant force which can only be supplied during the touchdown. During the flight, gravity will pull the mass downwards and as there is no counter that is applicable, the body will go down unless it is stance. Hence, the controller will try to keep a constant stance phase. This makes sure neither potential nor kinetic energy is lost during locomotion.

As it can be seen from the figure 3.1, CoM moves along a horizontal line. This means that the total force along the vertical direction is zero on the body. Therefore, the dynamic differential equation of the CoM could be obtained as

$$\begin{bmatrix} \dot{x_c} \\ \dot{z_c} \end{bmatrix} = \begin{bmatrix} \dot{x_d} \\ 0 \end{bmatrix} \tag{3.1}$$

where the system is first order.

3.1.2 LIP Model Control

LIP model does not require a controller as it does not have an input that we can give to the system to control the desired speed or height in this case. But the selection of system parameters are important. The height of the model should be a distance where CoM can safely follow. If it is a distance longer than maximum leg length, it would be illogical to expect the quadruped to follow the trajectory in a stable sense. If this distance is too short, then some motors of the robot will have to use a lot of power to create the required forces on the ground that follows the trajectory. The sweet spot is the distance when both legs are around the same angle when standing straight. In our case, this was around 0.3 m.

The desired speed is also chosen by the characteristics of the motors we have on the quadruped. Considering the time to get one leg to in flight to stance position or applying the required forces in the stance phase, 1 m/s is giving the motors a suitable time to reposition themselves.

3.2 The Spring Loaded Inverted Pendulum Template

3.2.1 System Model and Dynamics

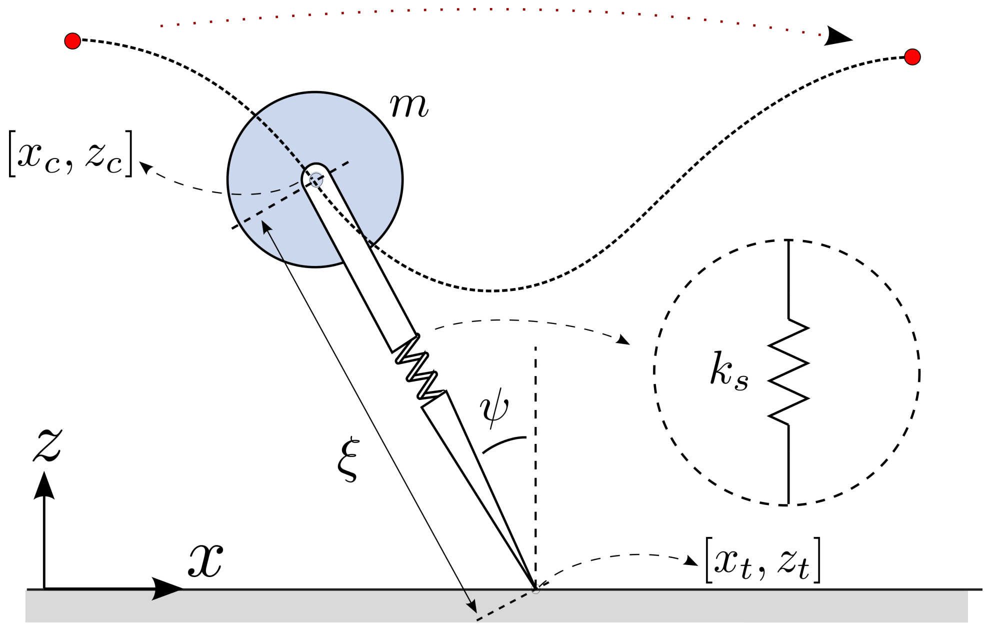

Figure 3.2: SLIP Model and related parameters

We model the SLIP dynamics the same as it is generally defined in the literature, consisting of a point mass m and a freely rotating massless leg, endowed with a linear spring pair of compliance k_s and rest length r_0. Throughout locomotion, the model alternates between stance and flight phases, which are further divided into the compression, decompression and ascent, descent subphases, respectively. These phases can be easily observed at the figure 3.3. In addition to the phases, four important events

Variable	Definition
$[x_c, z_c]$	SLIP CoM of body position (in W)
$[z_d, \dot{x_d}]$	Desired SLIP CoM height and velocity (in W)
$[x_t, z_t]$	SLIP toe position (in W)
$[\xi, \psi]$	SLIP leg length and angle
k_s	SLIP leg stiffness
r_0	SLIP leg rest length
m	Total body mass

Table 3.2: Parameters for SLIP model

define discrete transitions between these sub phases: touchdown, bottom, liftoff, and apex. During flight, the body is assumed to be a projectile acted upon by gravity, whereas in stance, the toe is assumed to be fixed on the ground and the mass feels radial forces generated by the leg. An illustration of the SLIP can be seen in figure 3.2 where the parameters of in the figure can be found in more detail in table 3.2.

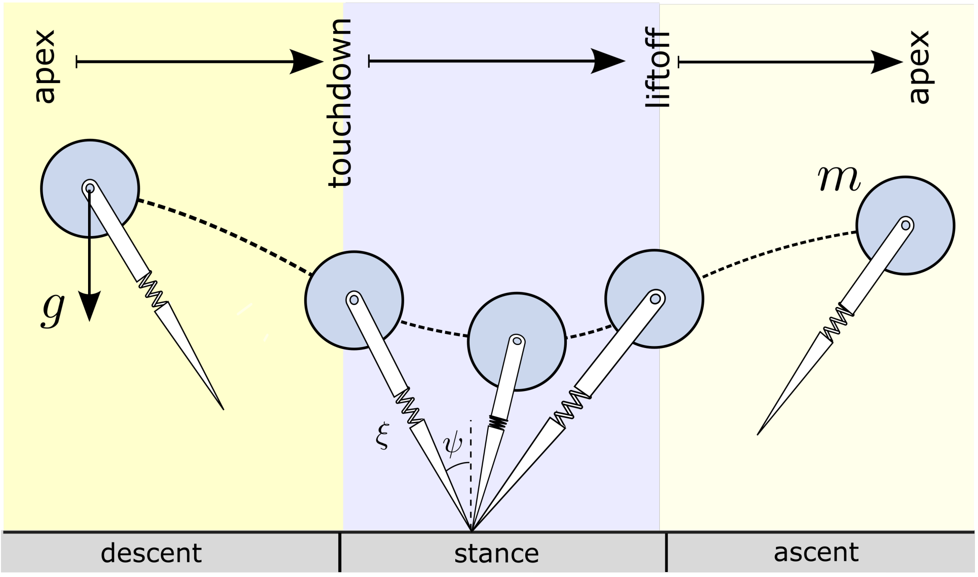

Figure 3.3: SLIP phases visualized

The state

$$S_{SLIP} = \begin{bmatrix} x_c & y_c & \dot{x_c} & \dot{y_c} & x_t & y_t \end{bmatrix} \tag{3.2}$$

is used in the different system equations in different states. SLIP model has 4 events. 1) *apex event* has the conditions

$$\dot{y}_c = 0 \tag{3.3}$$

$$\dot{y}_c \to 0^+ \tag{3.4}$$

that need to be satisfied to signal a successful gait behavior. 2) *fall down event* signals a failure and has the condition

$$y_c < 0 \tag{3.5}$$

to show that the body hit the ground. 3) *touchdown event* requires

$$y_t = 0 \tag{3.6}$$

to end the first flight phase and start the stance phase. 4) *liftoff event*, which is the last event, has the condition

$$\ddot{y}_t > 0 \tag{3.7}$$

to be satisfied. Liftoff indicates the end of stance phase and start of second flight phase. These motions can also be witnessed in figure 3.3. As the model starts in the apex position, flight dynamics should be expressed as

$$\dot{S_{SLIP}} = \begin{bmatrix} \dot{x}_c & \dot{y}_c & 0 & g & \dot{x}_c, & \dot{y}_c \end{bmatrix} \tag{3.8}$$

and the toes are set to target angle of attack at the apex. This flight model makes sure that the toes are moving along with the CoM. Until liftoff event, stance dynamics is given by

$$\dot{S_{SLIP}} = \begin{bmatrix} \dot{x}_c \\ \dot{y}_c \\ -\frac{k_s}{m}(r_0 - \sqrt{(x_c - x_t)^2 + (y_c - y_t)^2}) \sin\psi \\ \frac{k_s}{m}(r_0 - \sqrt{(x_c - x_t)^2 + (y_c - y_t)^2}) \cos\psi - g \\ 0 \\ 0 \end{bmatrix}^T \tag{3.9}$$

where all the parameters can be found in table 3.2 and the rest of the motion till the apex will be another flight phase where the dynamics are the same as 3.8. The apex is a terminal event, which means that the next cycle starts from this point.

3.2.2 SLIP Model Control

One of the first things to decide for the controller of SLIP is the touchdown angle for the leg. At the apex of the flight phase, a new touchdown angle shall be decided to further maximize the stability of the gait. Raibert's heuristic method

$$x_{f0} = \frac{\dot{x_c} T_s}{2} \tag{3.10}$$

$$T_s = T_{s_i}(1 + (z_d - z_c) - (\dot{x_d} - \dot{x_c})) \tag{3.11}$$

where x_{f0} is the forward displacement of the foot with respect to the center of mass, $\dot{x_c}$ is the velocity of center of mass, T_s is the stance period, T_{s_i} is the initial stance period, is what we have used in this controller. This angle of touchdown selection plays a huge role in the stance period. Convergence of the periodic running behavior to the desired state varies greatly with the selection of this parameter.

The next is the control of energy levels throughout the gait. The system has a starting energy, and there is no loss of energy as no damping or friction exists. To control the height of the model, we can control the energy of the system. The desired energy of the model in the apex moment, is defined as

$$E_d = mgz_d \tag{3.12}$$

where E_d is the desired energy level, z_d is the desired apex height. When the model is in the apex level, we can calculate its current energy level

$$E_c = mgz_c \tag{3.13}$$

and the energy difference between desired and current state of the model

$$\Delta E = E_d - E_c \tag{3.14}$$

shall be injected to or taken out from the system. One of the easiest methods to do it is the variable stiffness method where at the maximum leg compression, a step change in stiffness is forced. This unrealistic approach is not the most efficient method there is, but it makes sure that the stable gait is achieved upon enforcing

$$k(t) = \begin{cases} k_s & \dot{z} < 0 \text{ (compression)} \\ k_s + K_{p_s}\Delta E & \dot{z} > 0 \text{ (decompression)} \end{cases} \tag{3.15}$$

during stance where K_{p_s} is the SLIP controller leg stiffness constant.

CHAPTER 4

PLANAR QUADRUPED

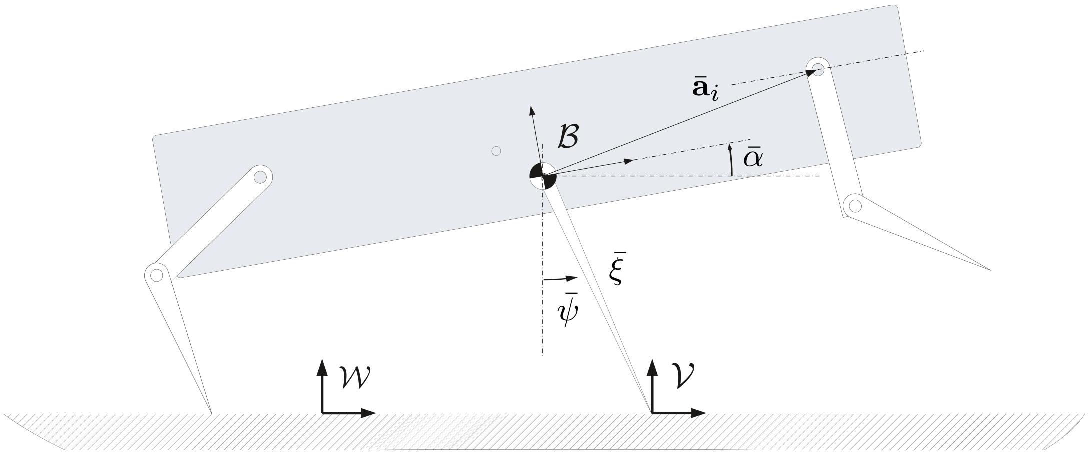

Figure 4.1: Planar quadruped model with realistic leg model

4.1 System Model and Dynamics

The quadruped model, whose illustration can be seen in figure 4.1, consists of a rigid body with inertia I and mass m, to which two legs with one motor on the hip, another on the knee are attached. The position and orientation of the body are represented by a body-fixed frame B with respect to an inertial world frame W. We also define a "virtual leg" extending from the body center of mass (COM) to a stationary point on the ground in coincidence with the virtual toe frame V having the same orientation as the world frame. Legs are considered massless during stance, with the toe position fixed on the ground at f_i, but very small toe masses $m_t << m$ are used to represent protraction dynamics during flight. Each leg is attached to the body through a pin joint with independently controllable torque τ_i, located at a_i in body coordinates. These

Variable	Definition
$c_b = [x_b, z_b]$	Body CoM position (in W)
a	Hip position (in B)
I	Body Inertia
α	Body pitch angle
F	Force variables (in W)
f	Toe position (in W)
m	Total body mass

Table 4.1: Parameters for planar quadruped model

parameters can be inspected in detail in 4.1.

For the sake of embedding SLIP which is 2D, we use a planar version of the quadruped where the robot can be imagined as if it was linked to an XY-stage therefore can only move in x-y directions and have pitch angle. In this scenario, the flight state vector

$$S_{qf} = \begin{bmatrix} x_b & z_b & \alpha & \theta_1 & \theta_2 & \theta_3 & \theta_4 & \dot{x_b} & \dot{z_b} & \dot{\alpha} & \dot{\theta_1} & \dot{\theta_2} & \dot{\theta_3} & \dot{\theta_4} \end{bmatrix}^T \tag{4.1}$$

is used in flight phase dynamics

$$\frac{\mathrm{d}}{\mathrm{d}t} S_{qf} = \begin{bmatrix} \dot{x_b} & \dot{z_b} & \dot{\alpha} & \dot{\theta_1} & \dot{\theta_2} & \dot{\theta_3} & \dot{\theta_4} & 0 & g & 0 & \tau_{FR}/I & \tau_{FL}/I & \tau_{RR}/I & \tau_{RL}/I \end{bmatrix}^T \tag{4.2}$$

to solve the system dynamics. Stance state vector

$$S_{qf} = \begin{bmatrix} x_b & z_b & \alpha & \dot{x_b} & \dot{z_b} & \dot{\alpha} \end{bmatrix}^T \tag{4.3}$$

is used during stance phase in

$$\frac{\mathrm{d}}{\mathrm{d}t} S_{qs} = \begin{bmatrix} \dot{x_b} \\ \dot{z_b} \\ \dot{\alpha} \\ (F_{x_{FR}} + F_{x_{FL}} + F_{x_{RR}} + F_{x_{RL}})/m \\ (F_{z_{FR}} + F_{z_{FL}} + F_{z_{RR}} + F_{z_{RL}})/m + g \\ \sum((f - c_b) \times F) \end{bmatrix} \tag{4.4}$$

to solve the system dynamics. Also, in the equation 4.4, the total torque on the body angle is calculated with

$$\sum(f-c_b)\times F=((f_{FR}-c_b)\times F_{FR}+(f_{FL}-c_b)\times F_{FL}+$$
$$\Rightarrow (f_{RR}-c_b)\times F_{RR}+(f_{RL}-c_b)\times F_{RL})/I \quad (4.5)$$

4.2 Control of the System

4.2.1 LIP Embedding Controller for Quadruped

As it was mentioned in the section 3.1.1, in an ideal case, LIP should not have a flight phase or should have an infinitesimally small flight phase so that model almost always stay in a stance phase indefinitely by changing legs one by one. However, in this implementation, those infinitesimally small time periods, are not infinitesimally small anymore. This is mainly because we do not want 3 or 4 legs to touch ground at any moment of the locomotion. It would slow down the movement. Hence, for each leg, there are two states: flight phase, stance phase.

Flight phase: Forward toe target position is defined as

$$\begin{bmatrix} f_x \\ f_z \end{bmatrix} = \begin{bmatrix} x_u+\rho\sin\phi \\ z_u-\rho\cos\phi \end{bmatrix} \quad (4.6)$$

where x_u is x-axis component of upper hips positional component and z_u is z-axis component of upper hips positional component, ρ is the length of virtual leg, ϕ is the angle of touchdown. This is a simple, yet effective method to calculates the target swing position. Then, inverse kinematics is used for calculating target angles of the legs. For this purpose, first the newly found position is transformed using

$$\begin{bmatrix} f_x^B \\ f_z^B \end{bmatrix} = {}^B T_W \begin{bmatrix} f_x \\ f_z \end{bmatrix} \quad (4.7)$$

from world coordinates to body coordinates, then inverse kinematics equations

$$\begin{bmatrix} \theta_{d_{knee}} \\ \theta_{d_{hip}} \end{bmatrix} = \begin{bmatrix} \arccos\left(\frac{f_x^{B^2}+f_z^{B^2}-l_1^2-l_2^2}{2l_1l_2}\right) \\ \arctan\left(\frac{f_z^B}{f_x^B}\right)-\arctan\left(\frac{l_1\sin\theta_{d_{knee}}}{l_2+l_1\cos\theta_{d_{knee}}}\right) \end{bmatrix} \quad (4.8)$$

are used to calculate angles required for this position. In equation 4.8, f_x^B is the new toe position in x-axis in body coordinates, f_z^B is the new toe position in z-axis in body coordinates, ${}^{B}T_W$ is the transformation matrix from body coordinates to world coordinates, $\theta_{d_{knee}}$ is the desired knee angle, $\theta_{d_{hip}}$ is the desired hip angle for the swing phase. After this point, the torques are calculated with a PD controller that is expressed as

$$\begin{bmatrix} \tau_{knee} \\ \tau_{hip} \end{bmatrix} = \begin{bmatrix} K_p(\theta_{d_{knee}} - \theta_{knee}) - K_d\dot{\theta}_{knee} \\ K_p(\theta_{d_{hip}} - \theta_{hip}) - K_d\dot{\theta}_{hip} \end{bmatrix} \tag{4.9}$$

where τ_{knee} is the torque that will be commanded to the knee motor, τ_{hip} is the motor torque that will be commanded to the hip motor, θ_{knee} is the current knee angle, θ_{hip} is the current hip angle, $\dot{\theta}_{knee}$ is the current knee angular velocity, $\dot{\theta}_{hip}$ is the current hip angular velocity.

The same method is applied for the both legs.

Stance phase: For this phase, a desired force is calculated with

$$F = \begin{bmatrix} F_x \\ F_z \end{bmatrix} = \begin{bmatrix} K_p(\dot{x}_d - \dot{x}_c) \\ K_p(z_d - z_c) + K_d(\dot{z}_d - \dot{z}_c) + mg \end{bmatrix} \tag{4.10}$$

where K_p is the proportional component of the stance controller, K_d is the derivative component of the stance controller, m is the mass and g is the gravity. Stance controller proportional and derivative components are found by manual tuning. In addition to these forces, another desired force

$$F_\theta = K_p\theta - K_d\dot{\theta} \tag{4.11}$$

is also added to balance the robot body. The force in 4.11 will be added to the front leg's z-axis forces and subtracted from the rear leg's z-axis forces. This will ensure the balance of the body. The commanded torques of the joints are calculated as

$$J = \begin{bmatrix} -l_1\sin(\theta + \theta_{hip}) - l_2\sin(\theta + \theta_{hip} + \theta_{knee}) & -l_2\sin(\theta + \theta_{hip} + \theta_{knee}) \\ l_1\cos(\theta + \theta_{hip}) + l_2\cos(\theta + \theta_{hip} + \theta_{knee}) & l_2\cos(\theta + \theta_{hip} + \theta_{knee}) \end{bmatrix} \tag{4.12}$$

where J is the jacobian of the front leg toe to the center of mass of the body. Combining all these equations in

$$\begin{bmatrix} \tau_{F_{hip}} \\ \tau_{F_{knee}} \\ \tau_{R_{hip}} \\ \tau_{R_{knee}} \end{bmatrix} = \begin{bmatrix} J_F & 0 \\ 0 & J_R \end{bmatrix}^T \begin{bmatrix} F_{F_x} \\ F_{F_z} + F_\theta \\ F_{R_x} \\ F_{R_z} - F_\theta \end{bmatrix} \tag{4.13}$$

results in the torques needed for the legs. In this equation τ_F is the torques of the front legs, τ_R is the torques of the rear legs, J_F is the jacobian of the front legs, J_R is the jacobian of the rear legs.

4.2.2 SLIP Embedding Controller for Quadruped

To control the system through embedding SLIP, a hybrid mode is used. This approach can be seen in figure 4.2. Here, the legs of the model are not 2 degree-of-freedom, but instead they are just a spring like the SLIP model. The parameters of the new model can be found in detail in table 4.2. Some of the physical parameters that are shared in the template SLIP model and quadruped model can also be found in table 4.3. As it was in the last section, this controller also has two phases: a flight phase where legs move to their new target angle in the air and a stance phase where legs apply force at the foot through torques in its leg joints. Here, flight phase takes a lot longer than LIP embedding controller.

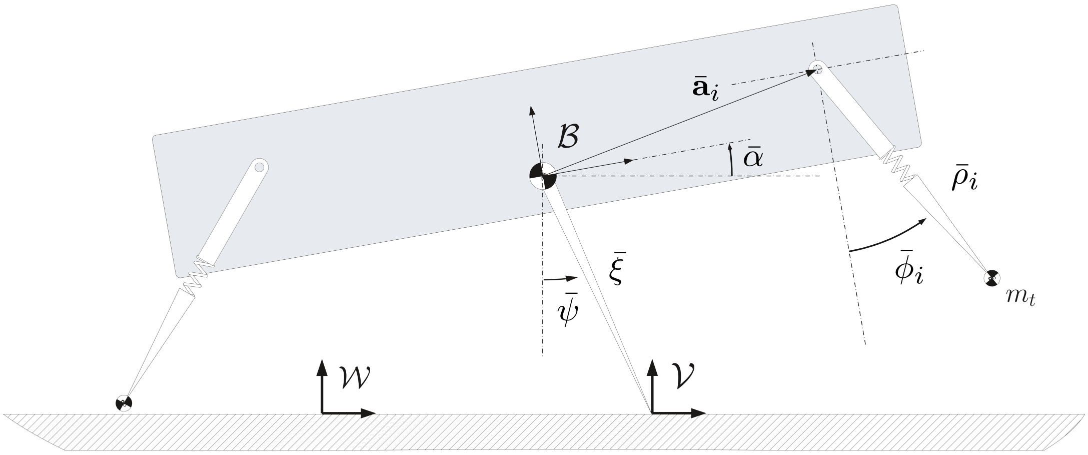

Figure 4.2: Planar quadruped mode with virtual SLIP leg model

Variable	Definition
$[\rho, \phi]$	Virtual leg length and angle

Table 4.2: Parameters for planar quadruped model with virtual leg

	ξ	k_s	m	a_1	a_2	I
SLIP	0.35	5000	10	-	-	-
Quadruped	0.35	5000	10	$[-0.24, 0]$	$[0.24, 0]$	0.26

Table 4.3: Physical Parameters for SLIP and quadruped models

Flight phase: Control of model in this phase is not different from the method that was proposed in the last chapter 4.2.1.

Stance phase: For this phase, let's consider polar coordinates stationed at the touch-down position for the stance duration of SLIP. This can be seen in figure 3.2. Then the relation between Cartesian coordinates and polar coordinates

$$\begin{bmatrix} \xi \\ \psi \end{bmatrix} = \begin{bmatrix} \sqrt{(x_c - f_x)^2 + (z_c - f_z)^2} \\ \text{atan2}((z_c - f_z), (x_c - f_x)) \end{bmatrix} \tag{4.14}$$

will be used to express stance dynamics as

$$\begin{bmatrix} \ddot{\xi} \\ \ddot{\psi} \end{bmatrix} = \begin{bmatrix} \xi\dot{\psi}^2 - g\cos\psi - (k_s/m)(\xi - r_0) \\ (-2\xi\psi + g\sin\psi)\xi \end{bmatrix} \tag{4.15}$$

so that the embedding of SLIP in the quadruped dynamics can be much smoother. However, before that, virtual leg variables for each leg shall be introduced. The leg vector $\mathbf{I}_i$ is defined as

$$\mathbf{I}_i = \mathbf{R}^T(\alpha)(\mathbf{f}_i - [x_c, z_c]^T) - \mathbf{a}_i \tag{4.16}$$

and these virtual leg vectors are transformed into polar coordinates. Using

$$\begin{bmatrix} \rho_i \\ \phi_i \end{bmatrix} = \begin{bmatrix} \sqrt{\mathbf{I}_{i,x}^2 + \mathbf{I}_{i,z}^2} \\ \text{atan2}(\mathbf{I}_{i,z}^2, \mathbf{I}_{i,x}^2) \end{bmatrix} \tag{4.17}$$

the transformation can be done. Utilizing the chain rule on jacobian

$$J = D_c\theta = \frac{\partial\theta}{\partial\phi}\frac{\partial\phi}{\partial c} + \frac{\partial\theta}{\partial\rho}\frac{\partial\rho}{\partial c} \tag{4.18}$$

we can embed SLIP dynamics in the planar quadruped dynamics. First virtual leg length partial derivatives with respective to polar SLIP state

$$\frac{\partial \phi}{\partial c} = \begin{bmatrix} \frac{\partial \phi_1}{\partial \xi} & \frac{\partial \phi_1}{\partial \psi} & \frac{\partial \phi_1}{\partial \alpha} \\ \\ \frac{\partial \phi_2}{\partial \xi} & \frac{\partial \phi_2}{\partial \psi} & \frac{\partial \phi_2}{\partial \alpha} \end{bmatrix} \tag{4.19}$$

where

$$\frac{\partial \phi_i}{\partial x} = \frac{1}{\rho^2} \mathbf{l}_i^T \begin{bmatrix} 0 & 1 \\ -1 & 0 \end{bmatrix} \frac{\partial \mathbf{l}_i}{\partial x} \tag{4.20}$$

and then virtual leg angle partial derivatives with respective to polar SLIP state

$$\frac{\partial \rho}{\partial c} = \begin{bmatrix} \frac{\partial \rho_1}{\partial \xi} & \frac{\partial \rho_1}{\partial \psi} & \frac{\partial \rho_1}{\partial \alpha} \\ \\ \frac{\partial \rho_2}{\partial \xi} & \frac{\partial \rho_2}{\partial \psi} & \frac{\partial \rho_2}{\partial \alpha} \end{bmatrix} \tag{4.21}$$

where

$$\frac{\partial \rho}{\partial x} = \frac{1}{\rho} \mathbf{l}_i^T \frac{\partial \mathbf{l}_i}{\partial x} \tag{4.22}$$

needs to be calculated. Here x is one of the polar SLIP state variables ξ, ψ or α, where $\frac{\partial \mathbf{l}_i}{\partial x}$ is calculated with

$$\frac{\partial \mathbf{l}_i}{\partial \psi} = \mathbf{R}^T(\alpha) \begin{bmatrix} \sin \psi \\ -\cos \psi \end{bmatrix} \tag{4.23}$$

$$\frac{\partial \mathbf{l}_i}{\partial \xi} = \mathbf{R}^T(\alpha) \xi \begin{bmatrix} \cos \psi \\ \sin \psi \end{bmatrix} \tag{4.24}$$

$$\frac{\partial \mathbf{l}_i}{\partial \alpha} = D_\alpha \mathbf{R}^T(\alpha) \left(\mathbf{f}_i - \mathbf{f}_v + \xi \begin{bmatrix} \sin \psi \\ -\cos \psi \end{bmatrix} \right) \tag{4.25}$$

Partial derivatives of hips to virtual leg angle

$$\frac{\partial \theta}{\partial \phi} = \begin{bmatrix} \frac{\partial \theta_{fu}}{\partial \phi_1} & \frac{\partial \theta_{fl}}{\partial \phi_1} & \frac{\partial \theta_{ru}}{\partial \phi_1} & \frac{\partial \theta_{rl}}{\partial \phi_1} \\ \\ \frac{\partial \theta_{fu}}{\partial \phi_2} & \frac{\partial \theta_{fl}}{\partial \phi_2} & \frac{\partial \theta_{ru}}{\partial \phi_2} & \frac{\partial \theta_{rl}}{\partial \phi_2} \end{bmatrix}^T = \begin{bmatrix} 1 & 0 & 0 & 0 \\ \\ 0 & 0 & 1 & 0 \end{bmatrix}^T \tag{4.26}$$

and partial derivatives of hips to virtual leg length

$$\frac{\partial\theta}{\partial\rho} = \begin{bmatrix} \dfrac{\partial\theta_{fu}}{\partial\rho_1} & \dfrac{\partial\theta_{fl}}{\partial\rho_1} & \dfrac{\partial\theta_{ru}}{\partial\rho_1} & \dfrac{\partial\theta_{rl}}{\partial\rho_1} \\ \\ \dfrac{\partial\theta_{fu}}{\partial\rho_2} & \dfrac{\partial\theta_{fl}}{\partial\rho_2} & \dfrac{\partial\theta_{ru}}{\partial\rho_2} & \dfrac{\partial\theta_{rl}}{\partial\rho_2} \end{bmatrix}^T = \begin{bmatrix} \dfrac{\partial\theta_{fu}}{\partial\rho_1} & \dfrac{\partial\theta_{fl}}{\partial\rho_1} & 0 & 0 \\ \\ 0 & 0 & \dfrac{\partial\theta_{ru}}{\partial\rho_2} & \dfrac{\partial\theta_{rl}}{\partial\rho_2} \end{bmatrix} \tag{4.27}$$

where

$$\frac{\partial\theta_{fu}}{\partial\rho_1} = \frac{(l_1^2 - l_2^2)/\rho_1^2 + 1}{2l_1\sqrt{1 - \left(\dfrac{l_2^2 - l_1^2 - \rho_1^2}{-2l_1\rho_1}\right)^2}} \tag{4.28}$$

$$\frac{\partial\theta_{fl}}{\partial\rho_1} = \frac{\rho_1}{-l_1 l_2\sqrt{1 - \left(\dfrac{\rho_1^2 - l_1^2 - l_2^2}{-2l_1 l_2}\right)^2}} \tag{4.29}$$

$$\frac{\partial\theta_{ru}}{\partial\rho_2} = \frac{(l_1^2 - l_2^2)/\rho_2^2 + 1}{2l_1\sqrt{1 - \left(\dfrac{l_2^2 - l_1^2 - \rho_2^2}{-2l_1\rho_2}\right)^2}} \tag{4.30}$$

$$\frac{\partial\theta_{rl}}{\partial\rho_2} = \frac{\rho_2}{-l_1 l_2\sqrt{1 - \left(\dfrac{\rho_2^2 - l_1^2 - l_2^2}{-2l_1 l_2}\right)^2}} \tag{4.31}$$

are combined in equation 4.18 to calculate the jacobian. The force vector in SLIP polar coordinates using acceleration calculation from 4.15 is defined as

$$F = \begin{bmatrix} F_x \\ \\ F_z \\ \\ F_\alpha \end{bmatrix} = \begin{bmatrix} m\ddot{\xi} - K_{p_x}(x_c - x_b) - K_{d_x}(\dot{x}_c - \dot{x}_b) \\ \\ m\ddot{\psi} - K_{p_z}(z_c - z_b) - K_{d_z}(\dot{z}_c - \dot{z}_b) \\ \\ -K_{p_\alpha}\alpha - K_{d_\alpha}\dot{\alpha} \end{bmatrix} \tag{4.32}$$

(4.33)

given the condition that

$$F_z \leq 0 \tag{4.34}$$

which finally, is used in calculation of commanded torques

$$\tau = \mathbf{S}(J^T)^\dagger F \tag{4.35}$$

where $^+$ is the pseudo-inverse operator and **S** is the touchdown matrix which indicates whether the leg touches the ground. As the Jacobian matrix here is 4×3, we cannot take the inverse. Nevertheless, the pseudo inverse is sufficient for the same effect. Also, the selection matrix makes sure that even if a single leg touches the ground, the quadruped can still apply force if it is beneficial. However, we still wait for double stance for even better stability, as it was observed to perform better during the simulations.

CHAPTER 5

EXPERIMENTS

In this section, we will delineate the capability of the embedding controllers of the last section, by supporting with data from simulation studies during walking behavior. We believe that these data will prove the capability of the producing stable gait. After showing each controller on its own section, we will provide another study where a SLIP embedding controller is combined with a parallel compliant spring in the leg joints that stores the energy for liftoff.

5.1 LIP Embedding Controller in Planar Quadruped

Below plots are the experiment results of linear inverted pendulum embedding controller. Given a target of $(z_d = 0.35, \dot{x} = 1.0)$ starting from a state of $(z_d = 0.4, \dot{x} = 0.9)$, the controller tries to keep the CoM at the desired height and desired velocity constantly.

In figure 5.1a, we can observe that the controller keeps track of the desired velocity with small deviations during leg swaps. These deviations are less than $\%1$ of the desired speed, and they do not seem to be diverging, rather converging. The reason for selection of a highly stiff controller is that LIP should keep the state of the model close to the target state at all times. We can also observe that in figure 5.1b, CoM cannot keep a straight line, but rather move upwards and downwards in relatively small amounts. These periods are when leg swap happens. As we have mentioned before, we did not want more than 2 legs to touch the ground at the same time. This would result in lowered performance in higher speeds.

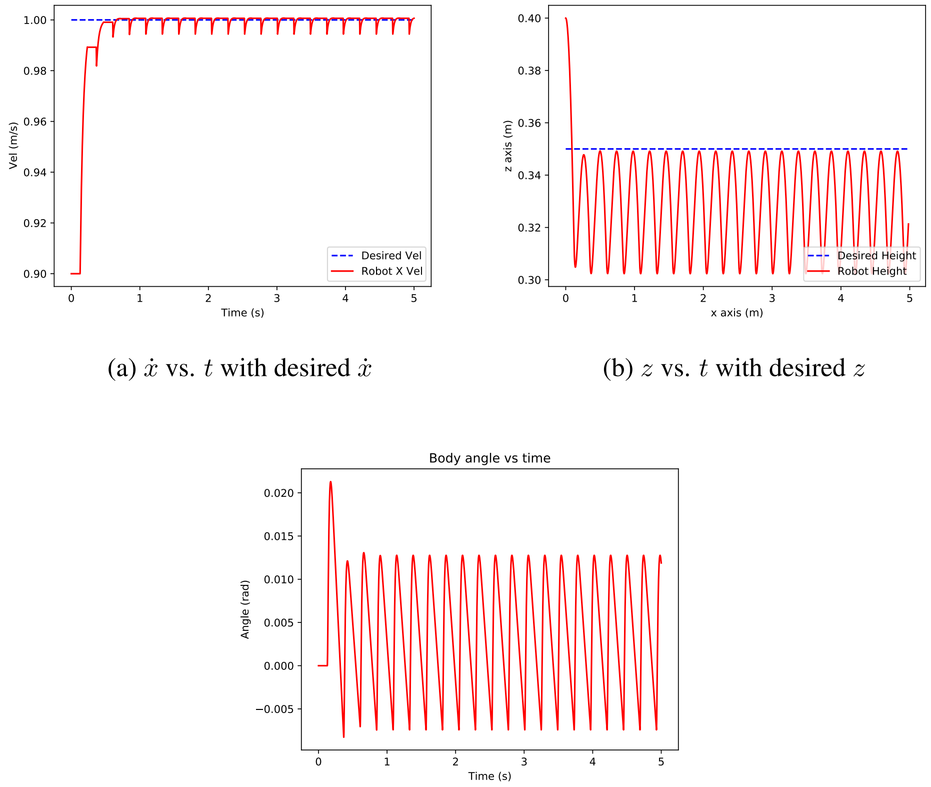

(a) $\dot{x}$ vs. t with desired $\dot{x}$

(b) z vs. t with desired z

(c) Change in body angle α

Figure 5.1: State variables during LIP embedded planar quadruped example simulation, starting from initial condition of $\dot{x} = 0.9$, $z = 0.4$ and targeting apex state of $\dot{x} = 1.0$, $z = 0.35$.

Figure 5.1c shows that the body angle during LIP embedding controller has oscillations. This is because in the flight phase, the control of the body angle is not possible. During the stance phase, the legs are used to keep the body angle steady. We can also see this in figure 5.2.

The torques at the start of stance phase is stepping, as we can spot it in figure 5.2. This is because the body is moving downwards during flight phase with the help of gravity. As soon as the legs touch the ground, the controller tries to stop the current state diverging from the target state. This results in a high torque output. Because we do not limit the motor torque, we can see impulses instead of saturations. The controller significantly lowers the output as the state of the quadruped gets closer to

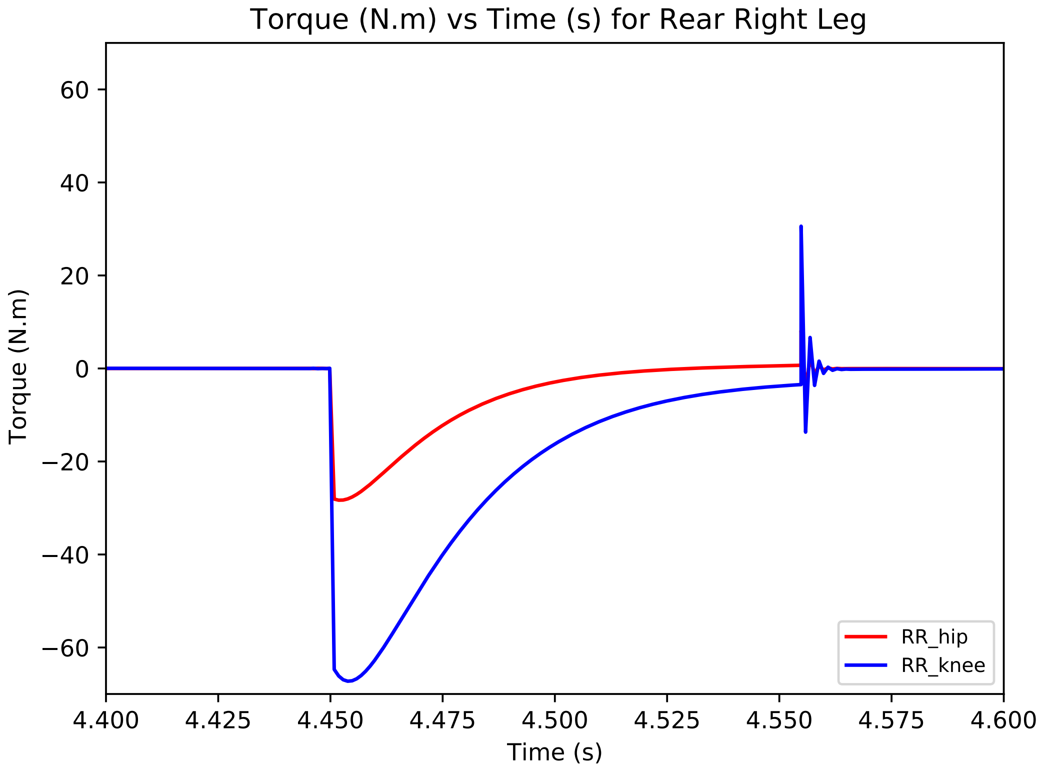

Figure 5.2: Rear Right leg output torques during LIP embedded planar quadruped example simulation last stance phase, with starting from initial condition of $\dot{x} = 0.9$, $z = 0.4$ and targeting apex state of $\dot{x} = 1.0$, $z = 0.35$

the target state. However, during the liftoff, motors torques oscillate to launch the robot from the ground.

5.2 SLIP Embedding Controller in Planar Quadruped

Below plots are the experiment results of spring linear inverted pendulum embedding controller in planar quadruped. Given a target of $(z_d = 0.35, \dot{x} = 1.0)$, starting from the initial condition of $\dot{x} = 0.9$, $z = 0.4$, the controller tries to apply SLIP motion to the CoM. Note that, SLIP by its nature does not enforce a constant speed or height. The apex state of the robot is the evidence of whether the system is converging to the desired state or not.

In figure 5.3a, it can be seen that the velocity of the apex converges to the desired

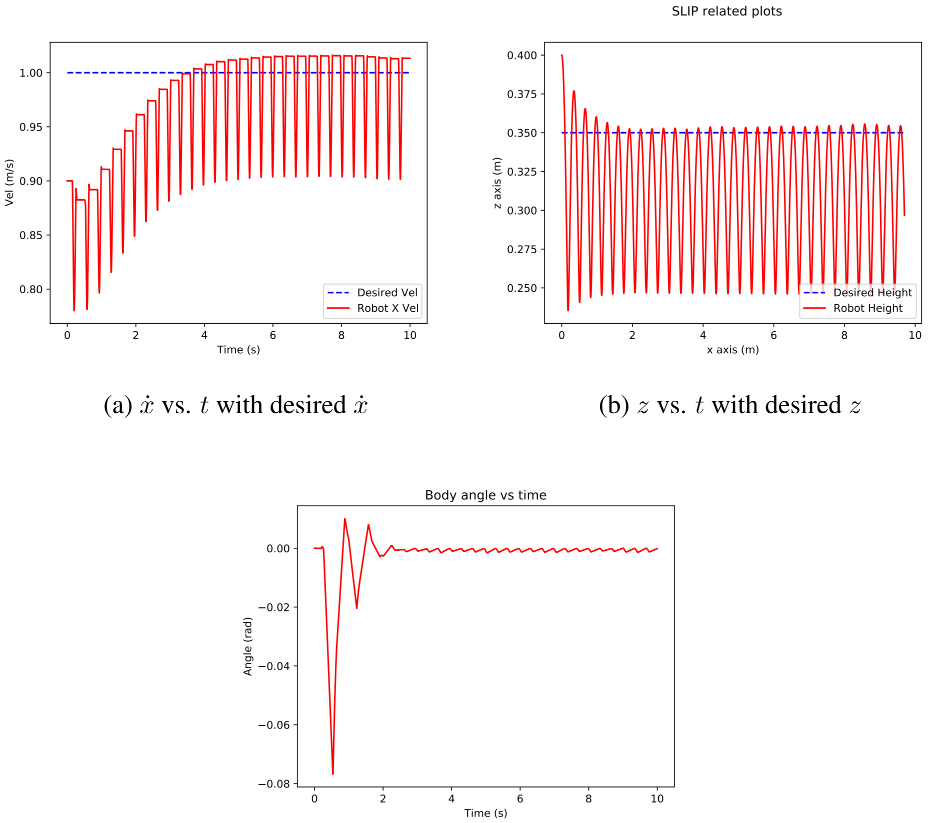

(a) $\dot{x}$ vs. t with desired $\dot{x}$

(b) z vs. t with desired z

(c) Change in body angle α

Figure 5.3: State variables during SLIP embedded planar quadruped example simulation, starting from initial condition of $\dot{x} = 0.9$, $z = 0.4$ and targeting apex state of $\dot{x} = 1.0$, $z = 0.35$.

velocity of $1m/s$. The deviations are a lot larger compared to the LIP embedding controller in figure 5.1a. This is expected behavior for this controller as LIP tries to keep a constant velocity, however, in SLIP only the apex state matters to keep the stability of the system. Also, considering the figure 5.3b which shows the height time relation of the CoM of the quadruped body, we can say that clearly see the motion of the body throughout the time period, and it is important to visualize the gait for understanding the difference between LIP and SLIP motions. We can notice larger oscillations for the CoM when compared with 5.1b. Another important plot that we should pay attention here is the figure 5.3c. When compared to the figure 5.1c, we can see larger oscillations as expected. The body can be subject to harsh changes in body angle to keep embedding SLIP template in this model, especially during the start of stance after a longer flight phase. However, the controller manages to keep the oscillations at much larger magnitude after a more stable gait is achieved.

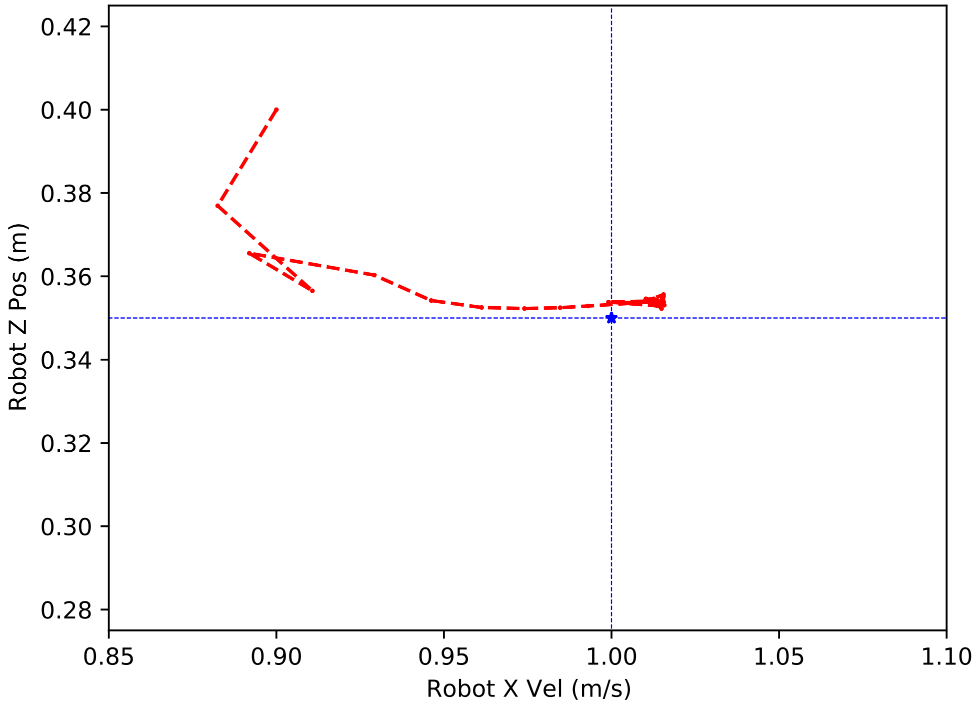

Figure 5.4: $\dot{x}$ vs. z with desired apex state in SLIP embedded planar quadruped example simulation, starting from initial condition of $\dot{x} = 0.9$, $z = 0.4$ and targeting apex state of $\dot{x} = 1.0$, $z = 0.35$

Another important figure that can be inspected to capture the stability of the system is the figure 5.4. Although the figure shows $\dot{x}$ vs z, it only has the data of the apex moments of the motion. This gives a better understanding of the system's convergence. In this figure, it is observed that quadruped follows quite close relations with the position and speed values of SLIP model. The target is marked with a star marker. Even though the system start from a far point, it converges to a point which is close to the desired state. This indicates that the gait is becoming more stable after some time.

The output torques after the locomotion is converged to a stable gait can be seen in figure 5.5. This figure by itself does mean anything. But it will make a lot more sense

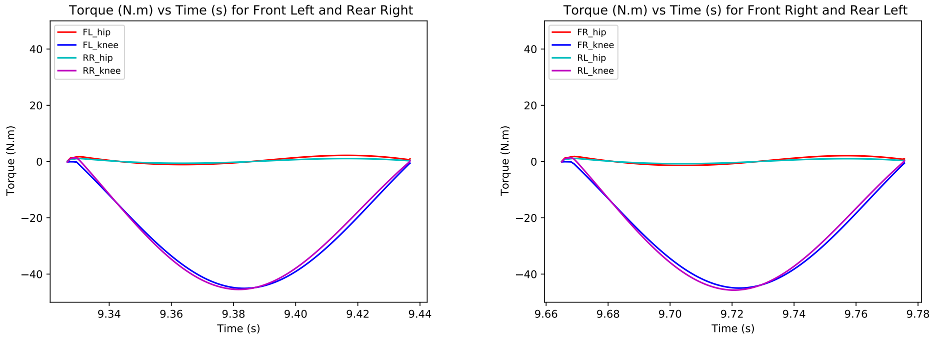

(a) Front Left and Rear Right legs' knee and hip output torques

(b) Front Right and Rear Left legs' knee and hip output torques

Figure 5.5: Legs' knee and hip output torques during a single step after converging to a stable locomotion in SLIP embedded planar quadruped example simulation, starting from initial condition of $\dot{x} = 0.9$, $z = 0.4$ and targeting apex state of $\dot{x} = 1.0$, $z = 0.35$.

when it is compared to in the oncoming experiments. Nevertheless, we can see that almost all the work is done by the knee motors, and they follow a smooth increase in power towards the maximum compression of the virtual springs. From this point onwards, the torques gradually degrade till the liftoff of the toes from the ground.

As the convergence of the stable gait can be a little hard to see from the motion of the CoM, another useful plot is the figure 5.7 and 5.6. These plots show the difference of the state of the system at the apex to apex point and the desired state. As it can be spotted from the figure 5.6, the difference from the target state during the apex moments is getting lower and lower till a point where it just oscillates. This oscillation is around $\%1$ of the desired height, and we consider this to be a low variation. Hence, we can say that the system is converged to a point. Note that this point might or might not be that target state. But it is a close point in this case.

In addition to the figure 5.6, figure 5.7 can also give insight about the convergence of the system. Similarly, it also has oscillations that are lower than $\%1$ of the desired speed, and we believe that it has converged to a stable point.

For the purpose of proving the stability of the controller, we have generated a domain

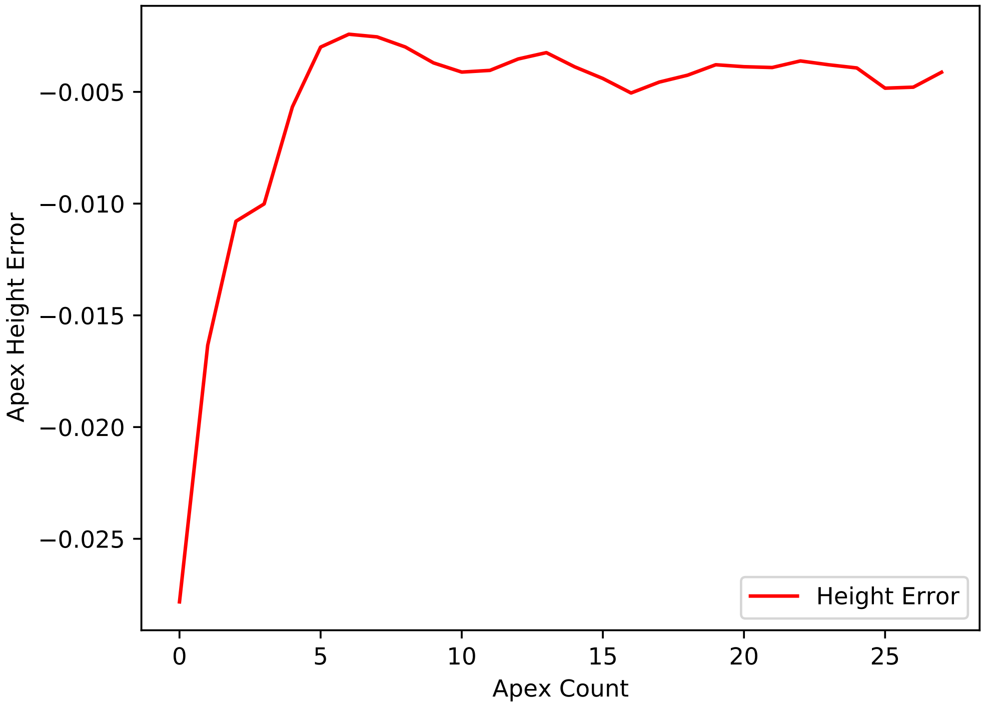

Figure 5.6: Robot CoM height moving average of apex points during SLIP embedded planar quadruped example simulation apex convergence, starting from initial condition of $\dot{x} = 0.9$, $z = 0.4$ and targeting apex state of $\dot{x} = 1.0$, $z = 0.35$

of attraction figure in 5.8. This shows that from varying different initial conditions, the controller can reach the target state in a feasible time. In this case, the apex state convergence should be within $\%10$ of the target state and timeout is 10 seconds. After 400 tests, we can see that the controller has the green area as initial states that model can go to the target state of targeted apex state of $\dot{x} = 1.0$, $z = 0.35$.

One last figure is whether the controller can reach different target states from different initial conditions. We have decided to select 4 points that are $\pm\%5$ of z_d and $\dot{x}_d$. We check whether the gait is converged to $\%10$ of the target state and timeout is 10 seconds. Even if one of the points fail, we consider that point is not satisfactory. These conditions resulted in the figure 5.9. We can see that the controller can handle different target state for a good portion of the space.

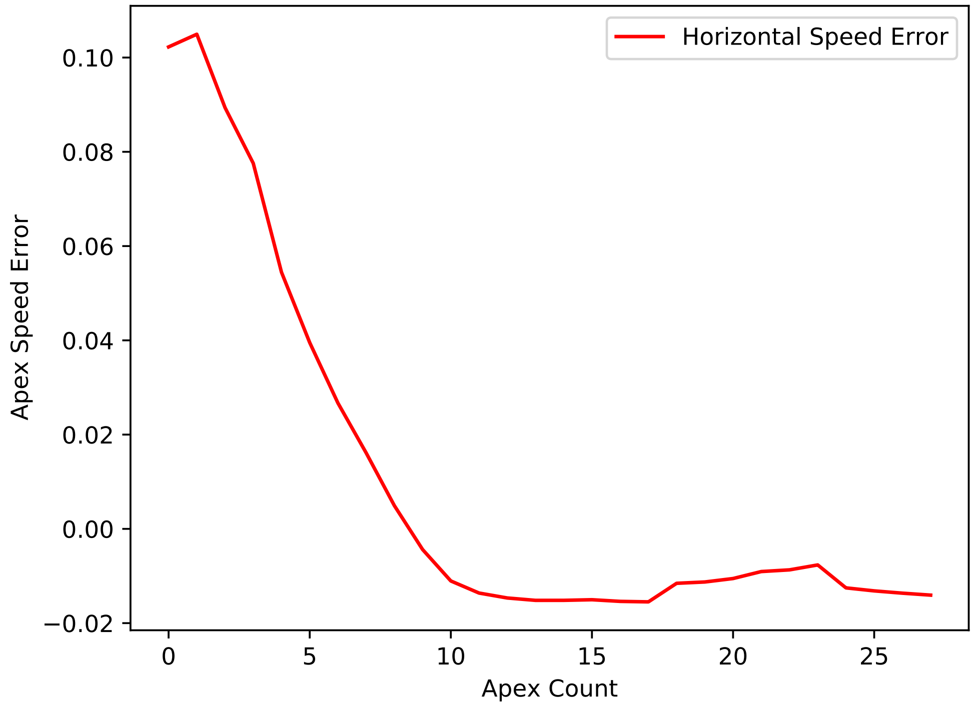

Figure 5.7: Robot CoM $\dot{x}$ moving average of apex points during SLIP embedded planar quadruped example simulation apex convergence, starting from initial condition of $\dot{x} = 0.9$, $z = 0.4$ and targeting apex state of $\dot{x} = 1.0$, $z = 0.35$

5.3 SLIP Embedding Controller in Planar Quadruped with Parallel Compliance

There have been many papers on how animals in nature implements the SLIP behavior, however, these animals also takes advantage of their compliant limbs. The efficiency of the SLIP lie in taking advantage of this compliant behavior. This section will try to prove this thesis in our experimental system.

First, let's define the radial forces that are applied on the leg so that we can find the force that can be stored on a compliant spring that will be added to the planar quadruped system. Considering the leg vector from 4.16, we transform

$$\mathbf{I}_W = {}^{W}T_B\mathbf{I} \tag{5.1}$$

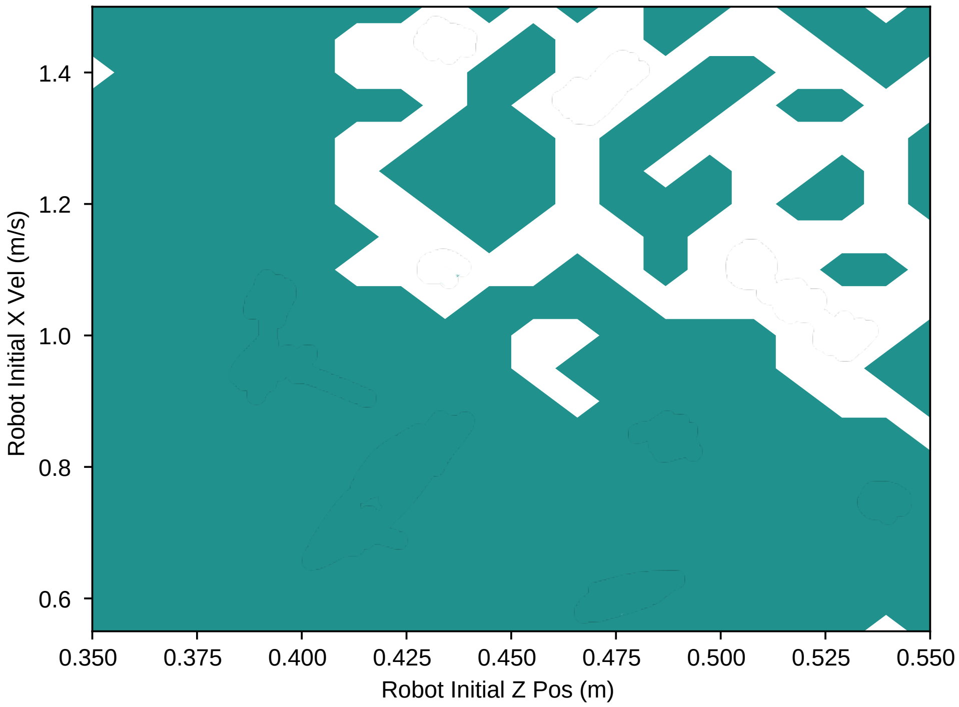

Figure 5.8: Convergence to a stable locomotion of different initial conditions. Initial $\dot{x}$ vs. initial z tested in SLIP embedded planar quadruped example simulation and targeted apex state of $\dot{x} = 1.0$, $z = 0.35$ with a timeout of 10 seconds. Green color indicates that starting from the given initial state, the robot is able to converge to the target state.

and use it in

$$F_R = \frac{\mathbf{I}_W F}{\|F\|} * F \tag{5.2}$$

to project the reaction force vector on to the leg vector, which results in the radial forces for the planar quadruped model. For a spring which has

$$F = kx \tag{5.3}$$

as its system model, the radial forces are in a linear relationship between the radial length and radial force. In the figure 5.10, the interaction between these forces and lengths can be seen. In the figure 5.10, the forces of that belong to legs are generated by the motors. However, spring stores the energy in and releases it back at the rest

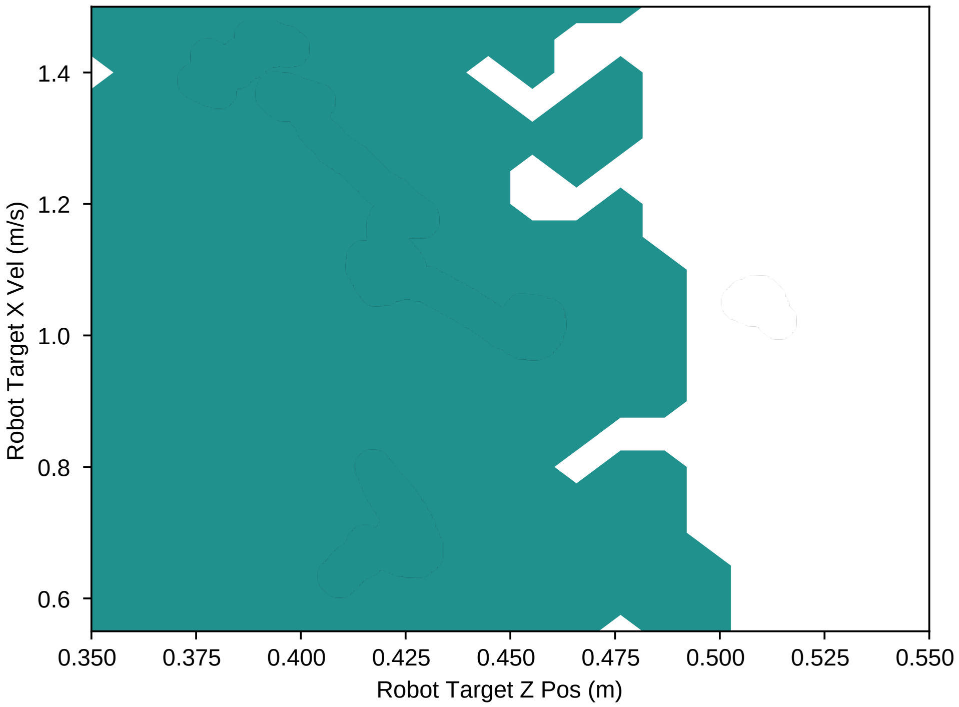

Figure 5.9: Target state analysis to a stable locomotion of different initial conditions. Initial $\dot{x}$ vs. initial z is $\pm\%$ 5 different from target condition. The cases are tested in SLIP embedded planar quadruped example simulation with a timeout of 10 seconds. Green color indicates that starting from the given initial states, the robot is able to converge to the target state.

length. If the motor has a parallel compliancy in the leg joint, the motors would only have to create the force required to move the force from the linear line of spring to the current required motor forces. This would result in a lot less torque requirements. In addition to this force, motors should also create a tangential force

$$F_T = F - F_R \tag{5.4}$$

which is the force that cannot be generated by the spring as these forces are perpendicular to it. This force can also be seen in figure 5.11. Another important observation from the figure 5.11 is that the tangential forces are dropping to 0 near the maximum compression of the spring. This is because at around this point in time, radial forces and the reaction forces are aligned. Hence, almost no tangential forces

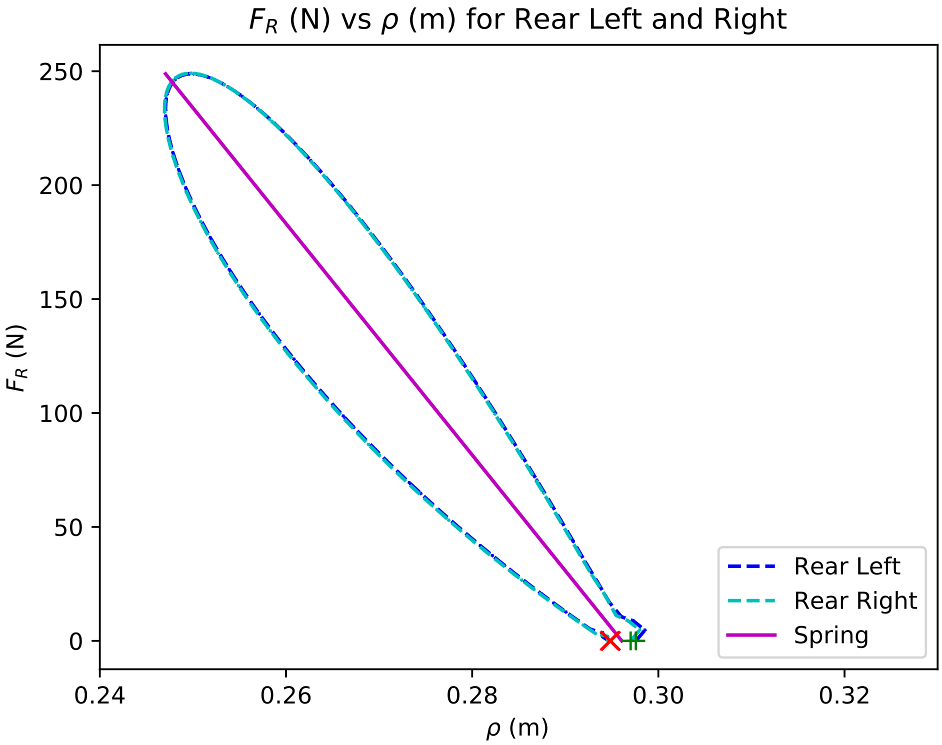

Figure 5.10: Rear Left and Right legs radial force vs. radial length, during SLIP embedded planar quadruped example simulation, radial force on the legs vs. radial length of the legs, starting from initial condition of $\dot{x} = 0.9$, $z = 0.4$ and targeting apex state of $\dot{x} = 1.0$, $z = 0.35$. Green plus is the start of stance, red cross is the end of stance.

are required. Therefore, unlike the radial forces, which are almost always required to keep the body floating, tangential forces are mostly required at the start and the end of the stance phase. In figure 5.12, we can see the torques of the planar quadruped with a parallel compliant joint, after converging to a stable gait during stance. When we compare it with 5.5a which is torques during SLIP embedding controller but without spring, we can clearly see a better distribution of the torques among the joints. Moreover, we can see that the torques near the maximum compression of the system is almost zero. This is again because the parallel spring compensates all the required forces to embed SLIP at this point and also cancels the gravity. Remembering the

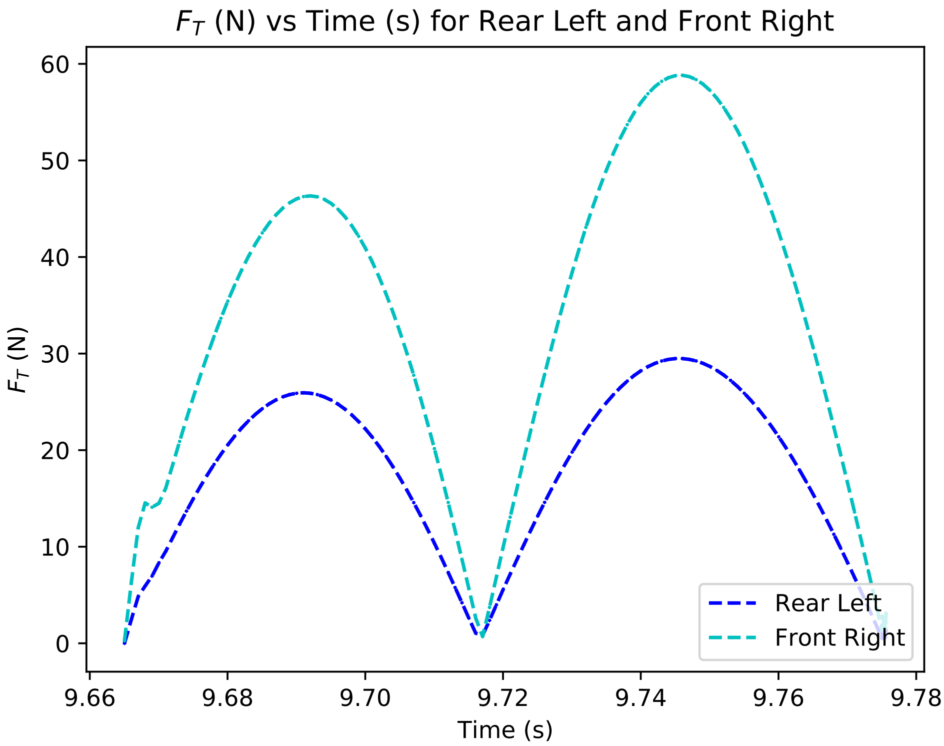

Figure 5.11: Front Right and Rear Left legs tangential force vs. time during SLIP embedded planar quadruped example simulation, radial force on the legs vs. radial length of the legs, starting from initial condition of $\dot{x} = 0.9$, $z = 0.4$ and targeting apex state of $\dot{x} = 1.0$, $z = 0.35$. Green plus is the start of stance, red cross is the end of stance.

jacobian formula from 4.12, motors try to create the torques by the following:

$$\tau = J(F_T + F_R - kx) \tag{5.5}$$

which means that when the better the system embeds a spring, the fewer torques it will require. If we imagine the system with real motors, we can also get a grasp of the power spent by the motors to get a clear picture of the efficiency of the control methods. The power spent at a single point in time can be calculated by:

$$P = V(\tau_{FR_{hip}} + \tau_{FR_{knee}} + \tau_{RL_{hip}} + \tau_{RL_{knee}}) \tag{5.6}$$

where P is the power spent in watts, V is the speed of the motors in rad/s and τ is the torque in Nm commanded by that joint. We can see the efficiency of the parallel

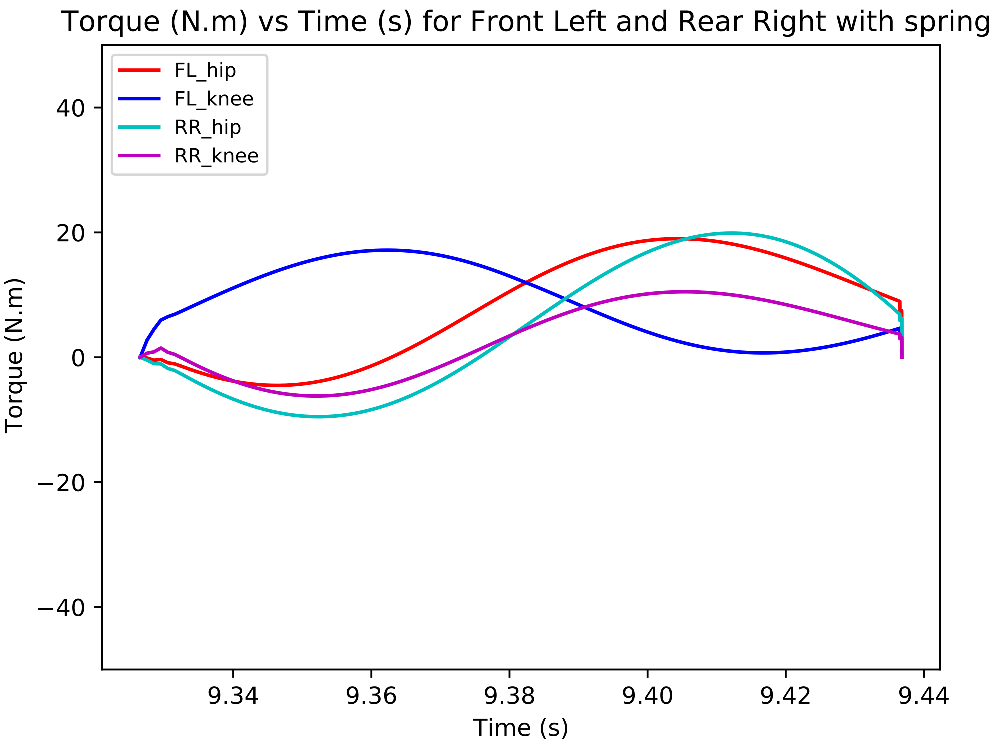

Figure 5.12: Front Left and Rear Right legs output torques during a single step after converging to a stable locomotion with a parallel spring placed in the physical legs in SLIP embedded planar quadruped example simulation, starting from initial condition of $\dot{x} = 0.9$, $z = 0.4$ and targeting apex state of $\dot{x} = 1.0$, $z = 0.35$

compliant joints in the figure 5.13 where the power spent by the planar quadruped with different controllers' is plotted. Although the SLIP embedding controller with spring seemed to be spending more power at the start and end, during most of the time, it spends a lot less than the version without the spring. This is because at the start and end of stance, the quadruped motion is far from the SLIP model. Hence, we see a lot more energy is pumped to the system to make sure the template is followed. In addition to this, similar to figure 5.12 and 5.11, near maximum compression, the power spent drops as the motors' speed lowers and the spring follows a very close relation to the template model.

Another figure that gives insight regarding the efficiency of the methods is the total power figure 5.14. This plot shows that amount of power spent from that start of a

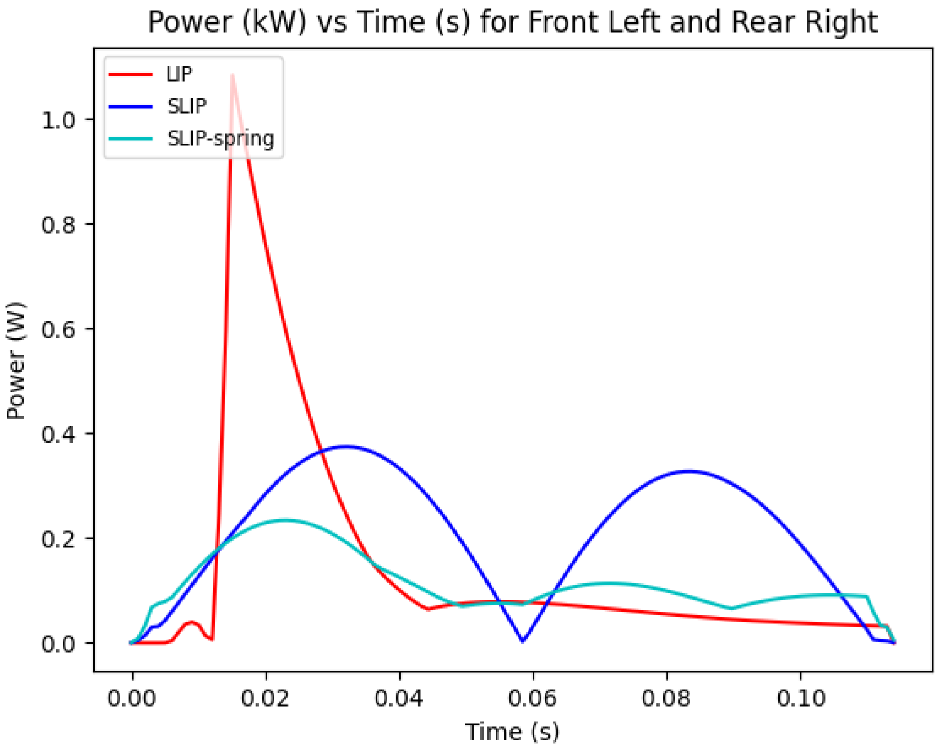

Figure 5.13: Power spent by motors during a single step after converging to a stable locomotion with & without a parallel spring placed in the physical legs in SLIP embedded planar quadruped example simulation, starting from initial condition of $\dot{x} = 0.9$, $z = 0.4$ and targeting apex state of $\dot{x} = 1.0$, $z = 0.35$

stance period till the end of it. We can see that LIP model start with a high power consumption and that is followed by a stable low consumption which can also be referred from the figure 5.13. However, we can see it clearly from figure 5.14 that SLIP embedded controller without the spring is a lot worse at efficiency than LIP embedded version. But with the parallel compliancy added to the system, we can observe a decrease in the total spent power by almost half.

Till this point, we were talking about efficiency, but in a single example. We can now increase the number of examples to see if this case is true in general. To achieve this, we need to use a metric for efficiency. We have selected

$$P_{avg} = P_{total}/t_{total} \tag{5.7}$$

as the average power metric to compare different controllers in different initial and

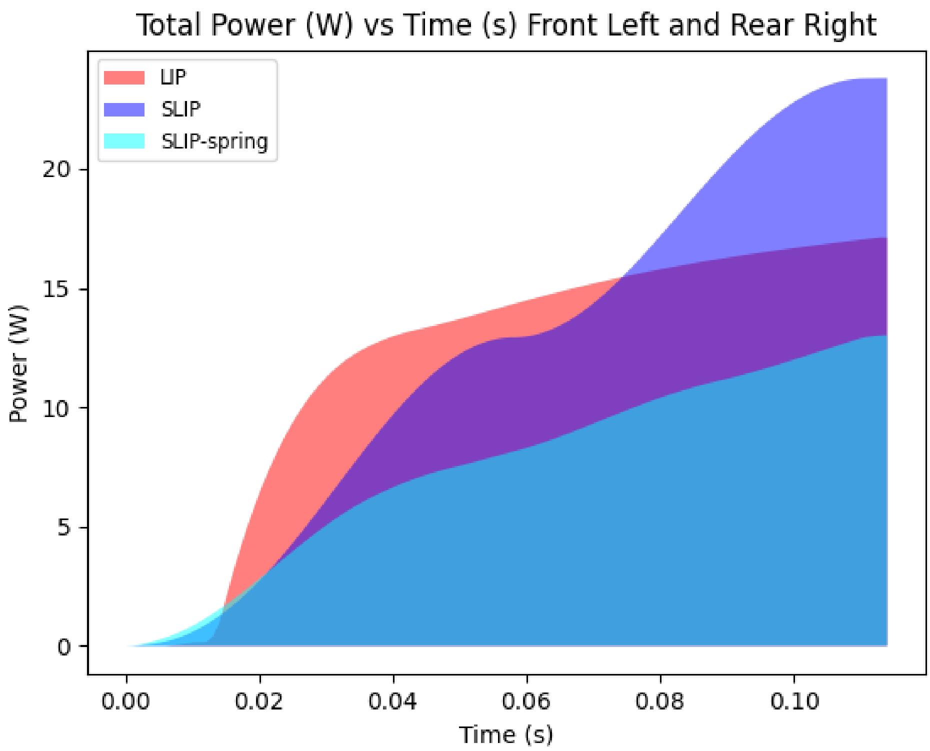

Figure 5.14: Total Power spent by motors during a single step after converging to a stable locomotion with & without a parallel spring placed in the physical legs in SLIP embedded planar quadruped example simulation, starting from initial condition of $\dot{x} = 0.9$, $z = 0.4$ and targeting apex state of $\dot{x} = 1.0$, $z = 0.35$

target conditions. In table 5.1 and 5.2, we have simulated used the initial state and target state as the same value, which ensured that all the controllers were close to the stable locomotion behavior.

In table 5.1 and 5.2, we notice that SLIP model with parallel compliancy make the planar quadruped model more efficient than other methods. We can see the most efficient methods in bold and in all the test cases, SLIP with parallel compliancy is the bold one. Sometimes LIP embedded controller and sometimes SLIP embedded controller were better than the other. As the target height increases or decreases a lot from some optimal point, LIP embedded controller performs worse overall. This is most likely because of the short flight phase and trying to keep CoM in a straight line with extended or retracted legs. All in all, SLIP embedded controller with parallel

Target State	LIP	SLIP	SLIP-spring	Target State	LIP	SLIP	SLIP-spring
0.35m 0.55m/s	57	68	**35**	0.35m 1.05m/s	67	75	**43**
0.36m 0.55m/s	67	75	**33**	0.36m 1.05m/s	77	83	**47**
0.37m 0.55m/s	76	83	**36**	0.37m 1.05m/s	88	93	**57**
0.38m 0.55m/s	83	89	**37**	0.38m 1.05m/s	95	94	**58**
0.39m 0.55m/s	74	85	**36**	0.39m 1.05m/s	84	87	**57**
0.35m 0.6m/s	58	68	**36**	0.35m 1.1m/s	68	75	**45**
0.36m 0.6m/s	68	76	**31**	0.36m 1.1m/s	78	84	**46**
0.37m 0.6m/s	78	84	**34**	0.37m 1.1m/s	89	93	**59**
0.38m 0.6m/s	85	90	**38**	0.38m 1.1m/s	97	92	**51**
0.39m 0.6m/s	76	85	**37**	0.39m 1.1m/s	85	87	**59**
0.35m 0.65m/s	59	69	**37**	0.35m 1.15m/s	69	77	**47**
0.36m 0.65m/s	69	76	**35**	0.36m 1.15m/s	80	86	**49**
0.37m 0.65m/s	79	84	**35**	0.37m 1.15m/s	90	96	**63**
0.38m 0.65m/s	86	90	**39**	0.38m 1.15m/s	96	92	**54**
0.39m 0.65m/s	77	86	**41**	0.39m 1.15m/s	84	82	**53**
0.35m 0.7m/s	60	69	**38**	0.35m 1.2m/s	71	78	**49**
0.36m 0.7m/s	70	77	**35**	0.36m 1.2m/s	81	87	**54**
0.37m 0.7m/s	80	84	**36**	0.37m 1.2m/s	91	96	**56**
0.38m 0.7m/s	88	91	**38**	0.38m 1.2m/s	97	93	**61**
0.39m 0.7m/s	77	86	**37**	0.39m 1.2m/s	86	82	**54**
0.35m 0.75m/s	62	70	**40**	0.35m 1.25m/s	71	80	**52**
0.36m 0.75m/s	72	77	**34**	0.36m 1.25m/s	81	89	**57**
0.37m 0.75m/s	82	86	**37**	0.37m 1.25m/s	91	99	**64**
0.38m 0.75m/s	88	92	**49**	0.38m 1.25m/s	99	94	**68**
0.39m 0.75m/s	79	87	**41**	0.39m 1.25m/s	86	81	**55**
0.35m 0.8m/s	63	71	**42**	0.35m 1.3m/s	73	82	**55**
0.36m 0.8m/s	72	78	**35**	0.36m 1.3m/s	83	92	**62**
0.37m 0.8m/s	82	85	**38**	0.37m 1.3m/s	93	101	**71**
0.38m 0.8m/s	90	92	**44**	0.38m 1.3m/s	99	95	**71**
0.39m 0.8m/s	78	86	**39**	0.39m 1.3m/s	88	82	**62**

Table 5.1: Average power usage of the different controllers in Watts, 1st batch of experiments. In these simulations, target state and initial state are chosen the same. Bold number is the most efficient controller in that test case.

Target State	LIP	SLIP	SLIP-spring	Target State	LIP	SLIP	SLIP-spring
0.35m 0.85m/s	63	71	**40**	0.35m 1.35m/s	74	83	**61**
0.36m 0.85m/s	74	79	**36**	0.36m 1.35m/s	84	94	**69**
0.37m 0.85m/s	83	87	**43**	0.37m 1.35m/s	94	103	**70**
0.38m 0.85m/s	90	92	**42**	0.38m 1.35m/s	100	95	**63**
0.39m 0.85m/s	80	87	**44**	0.39m 1.35m/s	88	83	**59**
0.35m 0.9m/s	64	72	**46**	0.35m 1.4m/s	74	86	**64**
0.36m 0.9m/s	75	80	**38**	0.36m 1.4m/s	84	95	**63**
0.37m 0.9m/s	85	88	**42**	0.37m 1.4m/s	95	102	**67**
0.38m 0.9m/s	91	93	**43**	0.38m 1.4m/s	102	95	**66**
0.39m 0.9m/s	80	88	**53**	0.39m 1.4m/s	88	84	**56**
0.35m 0.95m/s	65	73	**45**	0.35m 1.45m/s	75	89	**67**
0.36m 0.95m/s	77	81	**43**	0.36m 1.45m/s	86	99	**73**
0.37m 0.95m/s	86	88	**44**	0.37m 1.45m/s	96	102	**76**
0.38m 0.95m/s	93	93	**53**	0.38m 1.45m/s	103	95	**73**
0.39m 0.95m/s	82	88	**56**	0.39m 1.45m/s	89	86	**65**
0.35m 1.0m/s	66	73	**45**	0.35m 1.5m/s	110	90	**67**
0.36m 1.0m/s	77	82	**45**	0.36m 1.5m/s	88	101	**77**
0.37m 1.0m/s	87	91	**46**	0.37m 1.5m/s	95	101	**79**
0.38m 1.0m/s	93	93	**52**	0.38m 1.5m/s	103	91	**68**
0.39m 1.0m/s	82	86	**50**	0.39m 1.5m/s	90	87	**68**

Table 5.2: Average power usage of the different controllers in Watts, 2nd batch of experiments. In these simulations, target state and initial state are chosen the same. Bold number is the most efficient controller in that test case.

compliancy is much more efficient.

For better interpretation of the table 5.1 and 5.2, we have plotted the heat map of average power spent during simulations.

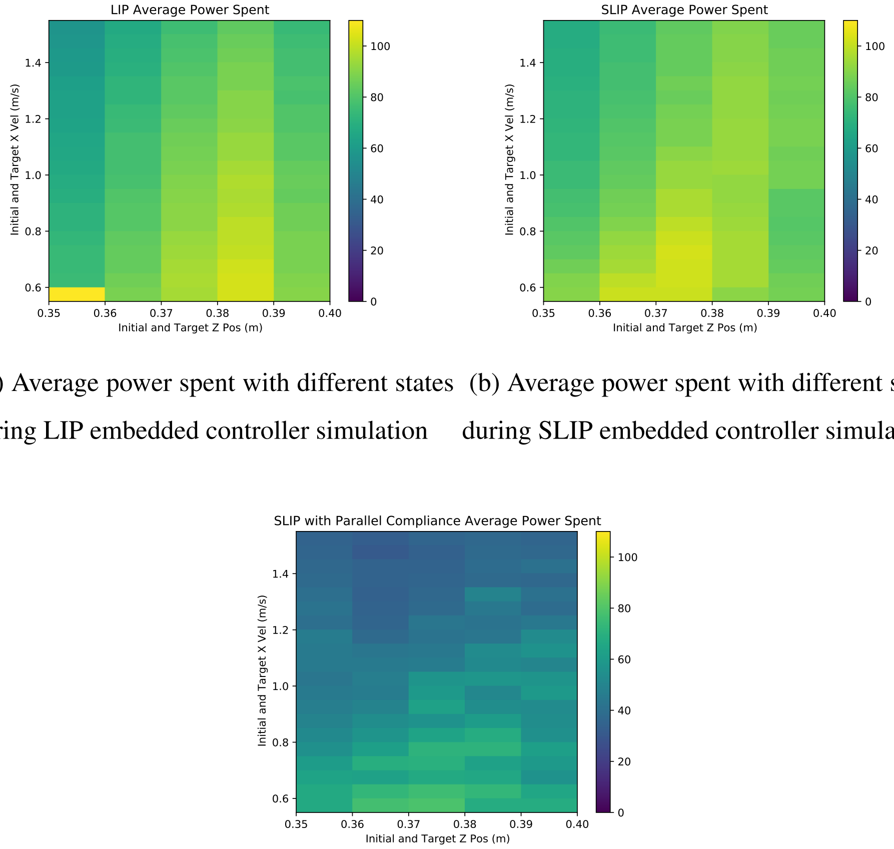

(a) Average power spent with different states during LIP embedded controller simulation

(b) Average power spent with different states during SLIP embedded controller simulation

(c) Average power spent with different states during SLIP embedded controller with parallel compliant joints simulation

Figure 5.15: Average power spent heat map of different controller for different initial and target states

In figure 5.15, we show the average power spent of different controller with different initial and target states. Figure 5.15a, 5.15b and 5.15c have different scales due to the fact that the maximum average power spent for each controller is different. When inspected one by one, each plot shows a similar result: low height, high speed means in less energy.

The last conclusion is not the proof of efficiency of the controller. Therefore, we have chosen a different method to show it: the differences of average power spending of each controller is shown in a heat map in figure 5.16.

In figure 5.16a, when the SLIP embedding controller is more efficient, the color becomes darker and when the LIP embedding controller is more efficient it becomes brighter. Looking at the plot, we can observe that LIP is more efficient in many of the test cases.

However, when we inspect 5.16b and 5.16c, we see that the scale never goes negative. This means that the SLIP embedding controller with parallel compliance is more efficient in every case. Hence, we can conclude that total power spent is a less with parallel compliance.

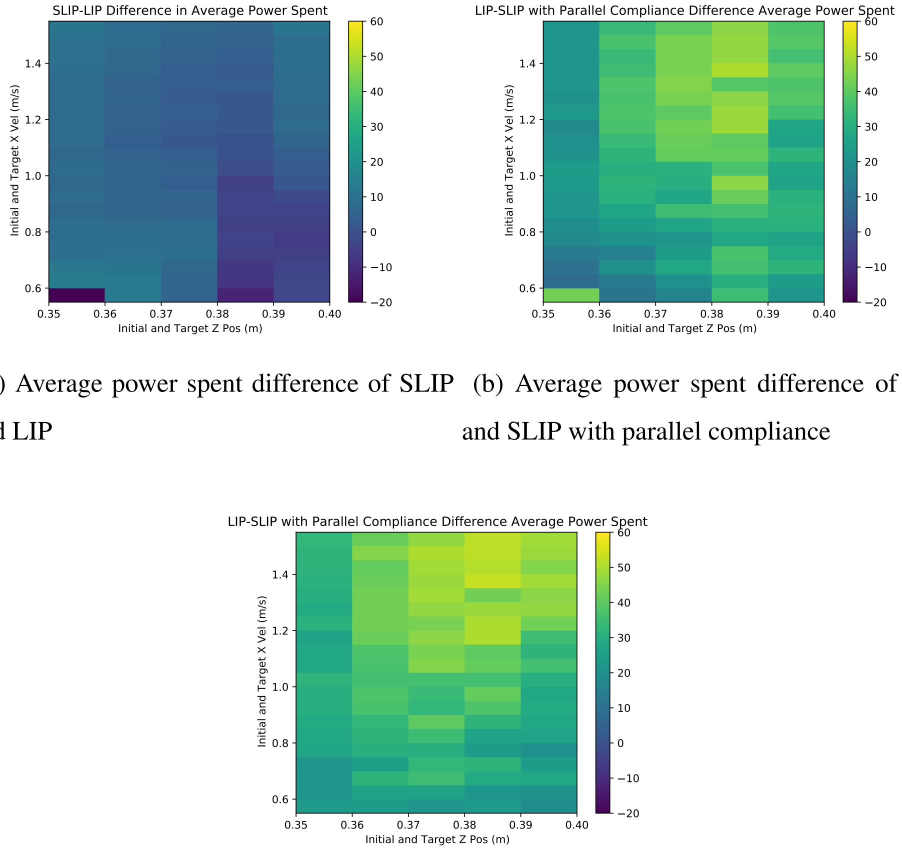

(a) Average power spent difference of SLIP and LIP

(b) Average power spent difference of LIP and SLIP with parallel compliance

(c) Average power spent difference of SLIP and SLIP with parallel compliance

Figure 5.16: Average power spent differences of different controller for different initial and target states

CHAPTER 6

CONCLUSIONS AND FUTURE WORK

In this thesis, we have introduced a new controller that provides stable gaits for the quadruped based on embedding spring loaded inverted pendulum as template model which captures the natural characteristic of the locomotion behavior. Using SLIP as the template model provides easy and simple access to many distinctive aspects of the locomotion. This template model offers many efficient and reliable method of control and by embedding this behavior to its full extent, we can take advantage of the new parallel compliant joint designs where the efficiency of the quadruped system can be increased drastically while also making sure of a stable gait without high computational effort.

We illustrate the powerful aspects of the technique by comparing it with different controllers embedded in a planar quadruped simulation. The models are expected to demonstrate a stable locomotion behavior, all the while provide the most efficient control that the embedded controllers can present. First linear inverted pendulum (LIP) is used as the embedding controller for the planar quadruped. This template is selected because it is adopted by many in recent times due to its simplicity and computational cheapness. Spring loaded inverted pendulum (SLIP) was the next controller that was embedded. This model is believed to be representing the motion of locomotion better than the LIP model, but it requires more work to embed on a quadrupedal model as this morphology does not feature such passively decoupled coordinates. We have proposed a method to fully capture the nature of SLIP in the model. We have then shown the same model with a spring on the leg joints to further boost the efficiency.

We have evaluated the proposed method in a walking scenario where the motion starts from an undesired state, and we wait till the gait convergences to the desired state.

First, the convergence to a stable gait, the domain of attraction and stability of the controller is shown on a single example. Next, The efficiency of the controllers are compared to the proposed method. A detailed example and different test results are provided to support this claim. This evaluation shows promising results when the controller is used with a parallel compliant joint, as the efficiency of the technique was higher than the other state-of-the-art methods.

6.1 Limitations and Future Work

This thesis introduced a novel control method for quadruped locomotion that takes advantage of the dynamics of natural walking behavior. Nevertheless, this thesis requires some assumptions to simplify the problem at hand. This section gives insight on how it can be improved further.

One of the most fundamental assumptions is that the system model is selected as two-dimensional to simplify the calculations and to show the results in a more focused manner. This choice indeed resulted in better evaluation of the proposed method, but it also made it require future work to embed it in a 3D model.

In the evaluation section, we have only focused on the comparison with the current template models. But currently, there are many other methods that can be used in comparison to further boost the validity of the proposed method.

Another work that can be done was to further optimize the motor torques using the null space of the jacobian matrix at the SLIP embedding controller. We have tuned the parameters by hand to find a good value, however, motor torques can be optimized using this method.

REFERENCES

[1] M. F. Silva and J. T. Machado, “A historical perspective of legged robots,” *Journal of Vibration and Control*, vol. 13, no. 9-10, pp. 1447–1486, 2007.

[2] G. Pratt, “Legged robots at mit: what’s new since raibert?,” *IEEE Robotics & Automation Magazine*, vol. 7, no. 3, pp. 15–19, 2000.

[3] M. LaBarbera, “Why the wheels won’t go,” *The American Naturalist*, vol. 121, no. 3, pp. 395–408, 1983.

[4] A. Agha, K. Otsu, B. Morrell, D. D. Fan, R. Thakker, A. Santamaria-Navarro, S.-K. Kim, A. Bouman, X. Lei, J. Edlund, M. F. Ginting, K. Ebadi, M. Anderson, T. Pailevanian, E. Terry, M. Wolf, A. Tagliabue, T. S. Vaquero, M. Palieri, S. Tepsuporn, Y. Chang, A. Kalantari, F. Chavez, B. Lopez, N. Funabiki, G. Miles, T. Touma, A. Buscicchio, J. Tordesillas, N. Alatur, J. Nash, W. Walsh, S. Jung, H. Lee, C. Kanellakis, J. Mayo, S. Harper, M. Kaufmann, A. Dixit, G. Correa, C. Lee, J. Gao, G. Merewether, J. Maldonado-Contreras, G. Salhotra, M. S. Da Silva, B. Ramtoula, Y. Kubo, S. Fakoorian, A. Hatteland, T. Kim, T. Bartlett, A. Stephens, L. Kim, C. Bergh, E. Heiden, T. Lew, A. Cauligi, T. Heywood, A. Kramer, H. A. Leopold, C. Choi, S. Daftry, O. Toupet, I. Wee, A. Thakur, M. Feras, G. Beltrame, G. Nikolakopoulos, D. Shim, L. Carlone, and J. Burdick, “Nebula: Quest for robotic autonomy in challenging environments; team costar at the darpa subterranean challenge,” 2021.

[5] M. Tranzatto, T. Miki, M. Dharmadhikari, L. Bernreiter, M. Kulkarni, F. Mascarich, O. Andersson, S. Khattak, M. Hutter, R. Siegwart, and K. Alexis, “Cerberus in the darpa subterranean challenge,” *Science Robotics*, vol. 7, no. 66, p. eabp9742, 2022.

[6] M. H. Raibert, “Trotting, pacing and bounding by a quadruped robot,” *Journal of Biomechanics*, vol. 23, pp. 79–98, 1990. International Society of Biomechanics.

[7] U. Saranli, M. Buehler, and D. E. Koditschek, "Rhex: A simple and highly mobile hexapod robot," *International Journal of Robotics Research*, vol. 20, pp. 616–631, 2001.

[8] M. Ahmadi and M. Buehler, "Controlled passive dynamic running experiments with the arl-monopod ii," *IEEE Transactions on Robotics*, vol. 22, no. 5, pp. 974–986, 2006.

[9] S. Seok, A. Wang, M. Y. Chuah, D. J. Hyun, J. Lee, D. M. Otten, J. H. Lang, and S. Kim, "Design principles for energy-efficient legged locomotion and implementation on the mit cheetah robot," *IEEE/ASME Transactions on Mechatronics*, vol. 20, no. 3, pp. 1117–1129, 2015.

[10] P.-A. Leziart, T. Flayols, F. Grimminger, N. Mansard, and P. Soueres, "Implementation of a reactive walking controller for the new open-hardware quadruped solo-12," *IEEE International Conference on Robotics and Automation (ICRA, under review)*, 2021.

[11] J. Di Carlo, P. M. Wensing, B. Katz, G. Bledt, and S. Kim, "Dynamic locomotion in the mit cheetah 3 through convex model-predictive control," in *2018 IEEE/RSJ International Conference on Intelligent Robots and Systems (IROS)*, pp. 1–9, 2018.

[12] O. A. Villarreal-Magaña, V. Barasuol, P. M. Wensing, and C. Semini, "Mpc-based controller with terrain insight for dynamic legged locomotion," *CoRR*, vol. abs/1909.13842, 2019.

[13] Z. Li, X. Cheng, X. B. Peng, P. Abbeel, S. Levine, G. Berseth, and K. Sreenath, "Reinforcement learning for robust parameterized locomotion control of bipedal robots," *CoRR*, vol. abs/2103.14295, 2021.

[14] Y. Yang, T. Zhang, E. Coumans, J. Tan, and B. Boots, "Fast and efficient locomotion via learned gait transitions," *arXiv*, 2021.

[15] D. Kim, J. D. Carlo, B. Katz, G. Bledt, and S. Kim, "Highly dynamic quadruped locomotion via whole-body impulse control and model predictive control," *ArXiv*, vol. abs/1909.06586, 2019.

[16] A. De and D. E. Koditschek, “The penn jerboa: A platform for exploring parallel composition of templates,” *ArXiv*, vol. abs/1502.05347, 2015.

[17] M. Hildebrand, “Motions of the Running Cheetah and Horse,” *Journal of Mammalogy*, vol. 40, pp. 481–495, 11 1959.

[18] A. W. English, “The functions of the lumbar spine during stepping in the cat.,” 1980.

[19] R. Blickhan and R. J. Full, “Similarity in multilegged locomotion: Bouncing like a monopode,” *Journal of Comparative Physiology A*, vol. 173, pp. 509–517, 1993.

[20] D. E. Koditschek and M. Bühler, “Analysis of a simplified hopping robot,” *The International Journal of Robotics Research*, vol. 10, no. 6, pp. 587–605, 1991.

[21] R. J. Full and D. E. Koditschek, “Templates and anchors: Neuromechanical hypotheses of legged locomotion on land,” *Journal of Experimental Biology*, vol. 202, pp. 3325–3332, 1999.

[22] U. Saranli, Ömür Arslan, M. M. Ankarali, and Ömer Morgül, “Approximate analytic solutions to non-symmetric stance trajectories of the passive spring-loaded inverted pendulum with damping,” *Nonlinear Dynamics*, vol. 62, pp. 729–742, 12 2010.

[23] G. Secer and U. Saranli, “Control of hopping through active virtual tuning of leg damping for serially actuated legged robots,” in *2014 IEEE International Conference on Robotics and Automation (ICRA)*, pp. 4556–4561, 2014.

[24] M. A. Sharbafi, M. J. Yazdanpanah, M. N. Ahmadabadi, and A. Seyfarth, “Parallel compliance design for increasing robustness and efficiency in legged locomotion–theoretical background and applications,” *IEEE/ASME Transactions on Mechatronics*, vol. 26, no. 1, pp. 335–346, 2021.

[25] E. Tanfener, S. S. Candan, A. E. Turgut, and U. Saranlı, “Modelling, Control and Design of a Clutched Parallel Elastically Actuated Articulated Robotic Leg Through Virtual Tunable Damping,” vol. Volume 7A: Dynamics, Vibration, and Control, 11 2020. V07AT07A021.

[26] M. Raibert, *Legged Robots that Balance*. Artificial Intelligence, MIT Press, 1986.

[27] R. M. Alexander, "Three uses for springs in legged locomotion," *The International Journal of Robotics Research*, vol. 9, no. 2, pp. 53–61, 1990.

[28] T. Mcgeer, "Passive dynamic walking," *The International Journal of Robotics Research*, vol. 9, pp. 62–82, 1990.

[29] T. A. McMahon and G. C. Cheng, "The mechanics of running: How does stiffness couple with speed?," *Journal of Biomechanics*, vol. 23, pp. 65–78, 1990. International Society of Biomechanics.

[30] J. W. Grizzle, G. Abba, and F. Plestan, "Asymptotically stable walking for biped robots: Analysis via systems with impulse effects," *IEEE Transactions on Automatic Control*, vol. 46, pp. 51–64, 2001.

[31] H. Komsuoglu, D. McMordie, U. Saranli, N. Moore, M. Buehler, and D. E. Koditschek, "Proprioception based behavioral advances in a hexapod robot," *Proceedings - IEEE International Conference on Robotics and Automation*, vol. 4, pp. 3650–3655, 2001.

[32] M. M. Ankarali and U. Saranli, "Control of underactuated planar pronking through an embedded spring-mass hopper template," *Autonomous Robots*, vol. 30, pp. 217–231, 2011.

[33] M. Buehler, R. Battaglia, A. Cocosco, G. Hawker, J. Sarkis, and K. Yamazaki, "Scout: a simple quadruped that walks, climbs, and runs," in *Proceedings. 1998 IEEE International Conference on Robotics and Automation (Cat. No.98CH36146)*, vol. 2, pp. 1707–1712 vol.2, 1998.

[34] M. Raibert, K. Blankespoor, G. Nelson, and R. Playter, "Bigdog, the rough-terrain quadruped robot," *IFAC Proceedings Volumes*, vol. 41, no. 2, pp. 10822–10825, 2008. 17th IFAC World Congress.

[35] C. Semini, V. Barasuol, J. Goldsmith, M. Frigerio, M. Focchi, Y. Gao, and D. Caldwell, "Design of the hydraulically-actuated, torque-controlled quadruped robot hyq2max," *IEEE/ASME Transactions on Mechatronics*, vol. PP, pp. 1–1, 10 2016.

[36] G. Bledt, M. J. Powell, B. Katz, J. Di Carlo, P. M. Wensing, and S. Kim, "Mit cheetah 3: Design and control of a robust, dynamic quadruped robot," in *2018 IEEE/RSJ International Conference on Intelligent Robots and Systems (IROS)*, pp. 2245–2252, 2018.

[37] F. Grimminger, A. Meduri, M. Khadiv, J. Viereck, M. Wuthrich, M. Naveau, V. Berenz, S. Heim, F. Widmaier, T. Flayols, J. Fiene, A. Badri-Sprowitz, and L. Righetti, "An open torque-controlled modular robot architecture for legged locomotion research," *IEEE Robotics and Automation Letters*, vol. 5, pp. 3650–3657, 4 2020.

[38] S. Kajita, F. Kanehiro, K. Kaneko, K. Yokoi, and H. Hirukawa, "The 3d linear inverted pendulum mode: a simple modeling for a biped walking pattern generation," in *Proceedings 2001 IEEE/RSJ International Conference on Intelligent Robots and Systems. Expanding the Societal Role of Robotics in the the Next Millennium (Cat. No.01CH37180)*, vol. 1, pp. 239–246 vol.1, 2001.

[39] S. Kajita, *Linear Inverted Pendulum-Based Gait*, pp. 905–922. Dordrecht: Springer Netherlands, 2019.

[40] A. Iqbal, S. Veer, and Y. Gu, "DRS-LIP: linear inverted pendulum model for legged locomotion on dynamic rigid surfaces," *CoRR*, vol. abs/2202.00151, 2022.

[41] H. Wang, H. Dong, L. He, Y. Shi, and Y. Zhang, "Design and simulation of lqr controller with the linear inverted pendulum," in *2010 International Conference on Electrical and Control Engineering*, pp. 699–702, 2010.

[42] L. Li, Z. Xie, X. Luo, and J. Li, "Trajectory planning of flexible walking for biped robots using linear inverted pendulum model and linear pendulum model," *Sensors*, vol. 21, no. 4, 2021.

[43] X. Xiong and A. D. Ames, "Orbit characterization, stabilization and composition on 3d underactuated bipedal walking via hybrid passive linear inverted pendulum model," in *2019 IEEE/RSJ International Conference on Intelligent Robots and Systems (IROS)*, pp. 4644–4651, 2019.

[44] O. Urbann, I. Schwarz, and M. Hofmann, “Flexible linear inverted pendulum model for cost-effective biped robots,” in *2015 IEEE-RAS 15th International Conference on Humanoid Robots (Humanoids)*, pp. 128–131, 2015.